ALGORITHM THEORETICAL BASIS DOCUMENT

GEOV2-AVHRR: Leaf Area Index (LAI), Fraction of Absorbed Photosynthetically Active Radiation (FAPAR) and Fraction of green Vegetation Cover (FCOVER) from LTDR AVHRR

THEIA-SP-44-0207-CREAF

Issue I2.50

Submission date: 24.09.2020

Start of the project: 18.09.2014

Organization name of lead contractor for this deliverable: CREAF

Book Captain: Aleixandre Verger (CREAF)
Contributing Authors: Marie Weiss (INRAE)
Frédéric Baret (INRAE)

Document Release Sheet

Book captain:	Aleixandre Verger		Sign Date 24.09.2020	
Approval:	Philippe Pacholczyk		Sign Date 24.09.2020	
Endorsement:			Sign	Date
Distribution:				

Change Record

Issue/Rev	Date	Page(s)	Description of Change	Release
	17.10.2014	All	First Issue	I1.00
I1.00	11.12.2014	All	Updated after internal review	I2.00
I2.00	19.01.2015	All	Updated after internal review	I2.10
I2.10	27.01.2015	All	Updated after internal review	I2.20
I2.20	29.04.2015	All	New calibration of the neural networks, adaptation of the temporal composition and improved quality assessment	I2.30
I2.30	31.07.2019	All	Description of spectral harmonization	I2.40
I2.40	24.09.2020	All	Editorial updates	I2.50

TABLE OF CONTENTS

LIST OF FIGURES

LIST OF TABLES

LIST OF ACRONYMS

ATBD	Algorithm theoretical based Document
AVHRR	Advanced Very High Resolution Radiometer
BELMANIP	BEnchmark Land Multisite ANalysis and Intercomparison of Products
BRDF	Bidirectional Reflectance Distribution Function
BS	Bare Soil
CACAO	Consistent Adjustment of Climatology to Actual Observations
CEOS	Committee for Earth Observation Satellite
CGLS	Copernicus Global Land Service
CNES	Centre National d'Études Spatiales (French Space Agency)
CREAF	Centre for Ecological Research and Forestry Applications
CYCLOPES	Carbon cYcle and Change in Land Observational Products from an Ensemble of Satellites
EBF	Evergreen Broadleaf Forest
ECV	Essential Climate Variable
FAPAR	Fraction of Absorbed Photosynthetically Active Radiation
FCOVER	Fraction of vegetation cover
GAC	Global Area Coverage
GAI	Green Area Index
GCOS	Global Climate Observation System
GEOCLIM	Climatology of Version 1 LAI, FAPAR, FCover VGT products
GEOV1	GEOLAND2 Version 1 product
GEOV2	GEOLAND2 Version 2 product
GTOS	Global Terrestrial Observation System
INRAE	Institut national de recherche pour l'agriculture, l'alimentation et l'environnement (National Research Institute for Agriculture, Food and Environment, France)
LAC	Local Area Coverage
LAI	Leaf Area Index
LPV	Land Product Validation group of CEOS
LTDR	Long Time Data Record
MODIS	Moderate Imaging Spectrometer
NDVI	Normalized Difference Vegetation Index
NIR	Near Infrared
NNT	Neural Network Technique
QC	Quality control indicator
QF	Quality flag
RMSE	Root Mean Square Error
SPOT	Satellite Pour l'Observation de la Terre
SWIR	Short Wave Infrared
SZA	Sun Zenith Angle
TOC	Top of Canopy

TSGF	Temporal Smoothing Gap Filling
VGT	VEGETATION instrument onboard SPOT satellite
VITO	Vlaamse Instelling voor Technologisch Onderzoek (Flemish Institute forTechnological Research), Belgium

1 BACKGROUND OF THE DOCUMENT

1.1 EXECUTIVE SUMMARY

This ATBD (Algorithm Theoretical Based Document) describes the proposed algorithm for Level 3 vegetation products derived at the global scale from AVHRR LTDR (Long Term Data Record) version 4 reflectance 1981-2019 series at 0.05° resolution (≈5.6km² at the equator) and every 10 days, with justification of the choices made. The considered products are the following set of biophysical variables: LAI and FAPAR that are essential climate variables (ECVs) as recognized by international organizations such as GCOS and GTOS. In addition, the FCOVER variable will be also generated since it corresponds to specific needs for some users.

The objective was to derive LAI, FAPAR and FCOVER variables as consistent as possible with the products derived from SPOT-VEGETATION and PROBA-V data in the framework of Copernicus Global Land Service (CGLS): the GEOV2-CGLS products (Baret et al. 2014; Verger et al. 2014). The same algorithm with minor adaptations to the specificities of the two datasets will be used for the generation of the two sets of GEOV2 products. The proposed methodology consists mainly in training neural networks (NNT) over existing CYCLOPES and MODIS products. Years 2003-2007 with concurrent CYCLOPES, MODIS and LTDR data available were used for training the NNT. The trained NNT were used to estimate GEOV2 LAI, FAPAR and FCOVER products from AVHRR normalized reflectances in the red and near infrared bands as provided in LTDR v4 series (Vermote and Claverie 2013; Vermote et al. 2010) at the daily time step, i.e. each time a AVHRR observation is available. Then, a specific gap filing and smoothing procedure was applied to generate smooth and continuous time series of products at the dekadal (10-day) time step. Finally, qualitative and quantitative quality indicators were associated to the products.

The comparison of the resulting products called GEOV2-AVHRR with the current version of Copernicus GEOV2-CGLS time series derived from VEGETATION and PROBA-V data demonstrates that they are very consistent, providing continuous time series of observations of LAI, FAPAR and FCOVER globally for the 1981-2019 time period, with continuation after 2019 with AVHRR data.

1.2 SCOPE AND OBJECTIVES

The GEOV2-AVHRR product is a global map of biophysical variables (FAPAR, LAI and FCOVER) derived from AVHRR LTDR data for the period 1981-2019 at 0.05° resolution (≈5.6km² at the equator) every ten days.
A first version of the product, called GEOV1-AVHRR, was developed from AVHRR LTDR version 3 data during the FP7 Geoland 2 project. The algorithm theoretical baseline description (ATBD) of this first product was produced by INRAE with the support of the CREAF laboratory (Baret et al. 2011). CNES developed the processing line and produced the first version of the product.
This first version was compared with the GEOV1-CGLS product prototyped by INRAE and CREAF. Some limitations were identified in GEOV1-AHRR product that needed to be corrected.

After this first analysis, it was decided to adapt the GEOV2-CGLS algorithm to the characteristics of the AVHRR products to generate GEOV2-AVHRR products.
The objective of this document is to provide a detailed description and justification of the algorithm proposed for version 2.0 of the algorithm based on daily AVHRR LTDR version 4 data to complement in a consistent way the existing GEOV2-CGLS products derived from the VEGETATION and PROBA-V sensors.

A quality assessment of the GEOV2-AVHRR products following CEOS/LPV recommendations is presented in [THEIA-RP-44-0281-CREAF].

1.3 CONTENT OF THE DOCUMENT

This ATBD document provides a description of the GEOV2-AVHRR algorithm including:

- The definition of the proposed products.
- The outline of the algorithm.
- A brief description of the AVHRR data from which the products will be derived.
- The inputs required and outputs provided by the algorithm
- The retrieval technique used. Neural network techniques will constitute the core of the operational algorithm, completed with dedicated data filtering and smoothing. A description of the quality indicators, including both qualitative and quantitative descriptors.

1.4 RELATED DOCUMENTS

1.4.1 Applicable documents

Document ID	Descriptor
CNES contract N°140570/00	CNES contracts scientific support of CREAF for the development and validation of the GEOV2-AVHRR products
THEIA-CT-44-0163-CNES	Scientific support requested

1.4.2 Output

Document ID	Descriptor
THEIA-SB-44-369-CNES	Product User Manual summarizing all information about GEOV2-AVHRR products
THEIA-RP-44-0281-CREAF	Validation Report describing the results of the scientific quality assessment of the GEOV2-AVHRR products

2 METHODOLOGY DESCRIPTION

2.1 OVERVIEW

The considered products correspond to actual vegetation biophysical variables that are defined below.

2.1.1 FAPAR

FAPAR corresponds to the fraction of photosynthetically active radiation absorbed by the canopy. The FAPAR value results directly from the radiative transfer model in the canopy which is computed instantaneously. It depends on canopy structure, vegetation element optical properties and illumination conditions. FAPAR is very useful as input to a number of primary productivity models based on simple efficiency considerations (Prince 1991). Most of the primary productivity models using this efficiency concept are running at the daily time step. Consequently, the product definition should correspond to the daily integrated FAPAR value that can be approached by computation of the clear sky daily integrated FAPAR values as well as the FAPAR value computed for diffuse conditions. To improve the consistency with other FAPAR products that are sometimes considering the instantaneous FAPAR value at the time of the satellite overpass under clear sky conditions (e.g. MODIS), a study investigated the differences between alternative FAPAR definitions (Baret et al. 2003). Results show that the instantaneous FAPAR value at 10:00 (or 14:00) solar time is very close to the daily integrated value under clear sky conditions. To keep a higher consistency with the FAPAR definition used in the CYCLOPES, and MODIS products, the instantaneous FAPAR value at 10:00 solar time under clear sky conditions (equivalent to black-sky conditions as defined also for albedo) was used.

FAPAR is relatively linearly related to reflectance values, and will be little sensitive to scaling issues. Note also that the FAPAR refers only to the green parts of the canopy.

2.1.2 Cover fraction (FCOVER)

It corresponds to one minus the gap fraction for nadir direction. FCOVER is used to separate vegetation and soil in energy balance processes, including temperature and evapotranspiration. It is computed from the leaf area index and other canopy structural variables and does not depend on variables such as the geometry of illumination as compared to FAPAR. For this reason, it is a very good candidate for the replacement of classical vegetation indices for the monitoring of green vegetation. Because of its quasi-linear relationship with reflectances, FCOVER will be only marginally scale dependent (Weiss et al. 2000). Note that similarly to LAI and FAPAR, only the green elements will be considered.

2.1.3 Leaf Area Index (LAI)

LAI is defined as half the developed area of photosynthetically active elements of the vegetation per unit horizontal ground area. It determines the size of the interface for exchange of energy (including radiation) and mass between the canopy and the atmosphere. This is an intrinsic canopy primary

variable that should not depend on observation conditions. LAI is strongly non linearly related to reflectance. Therefore, its estimation from remote sensing observations will be scale dependent (Garrigues et al. 2006; Weiss et al. 2000). Note that vegetation LAI as estimated from remote sensing will include all the green contributors such as the understory when existing under forests canopies. However, except when using directional observations (Chen et al. 2005), LAI is not directly accessible from remote sensing observations due to the possible heterogeneity in leaf distribution within the canopy volume. Therefore, remote sensing observations are rather sensitive to the 'effective' leaf area index, i.e. the value that provides the same diffuse gap fraction while assuming a random distribution of leaves. The difference between the actual LAI and the effective LAI may be quantified by the clumping index (Chen et al. 2005) that roughly varies between 0.5 (very clumped canopies) and 1.0 (randomly distributed leaves). Note that similarly to the other variables, the retrieved LAI is mainly corresponding to the green element: the correct term to be used would be GAI (Green Area Index) although we propose to still use LAI for the sake of simplicity.

2.2 THE RETRIEVAL ALGORITHM

2.2.1 Basic underlying assumptions

The objective is to develop an algorithm dedicated to the estimation of LAI, FAPAR and FCOVER from the AVHRR series of observations. The algorithm should provide improved products as compared to GEOV1-AVHRR although derived from the same sensors AVHRR/NOAA observations. These LAI, FAPAR and FCOVER products, called here GEOV2-AVHRR, aims to be consistent with GEOV2-CGLS products to ensure continuity. GEOV2-AVHRR should have the same temporal sampling frequency of 10 days. GEOV2-AVHRR capitalizes on the development and validation of already existing CYCLOPES and MODIS products, and the use of neural networks. The basic underlying assumption is that a strong link exists between AVHRR observations and the FUSED products resulting from the fusion of CYCLOPES and MODIS. Products should also be associated with quality flags as well as quantified uncertainties.

2.2.2 Outline

The GEOV2-AVHRR algorithm for the estimation of LAI, FAPAR, and FCOVER global time series (1981-2019) from AVHRR data consists of two main steps (Figure 1):

1. Neural networks are used to derive instantaneous estimates from LTRD AVHRR V4.0 top of the canopy directionally normalized reflectances in the red and near infrared spectral bands (Branch A, Figure 1).
2. Filtering, smoothing, gap filling and temporal compositing techniques are applied to ensure consistency and continuity of the LAI, FAPAR and FCOVER time course every 10 days (Branch B,.Figure 1).

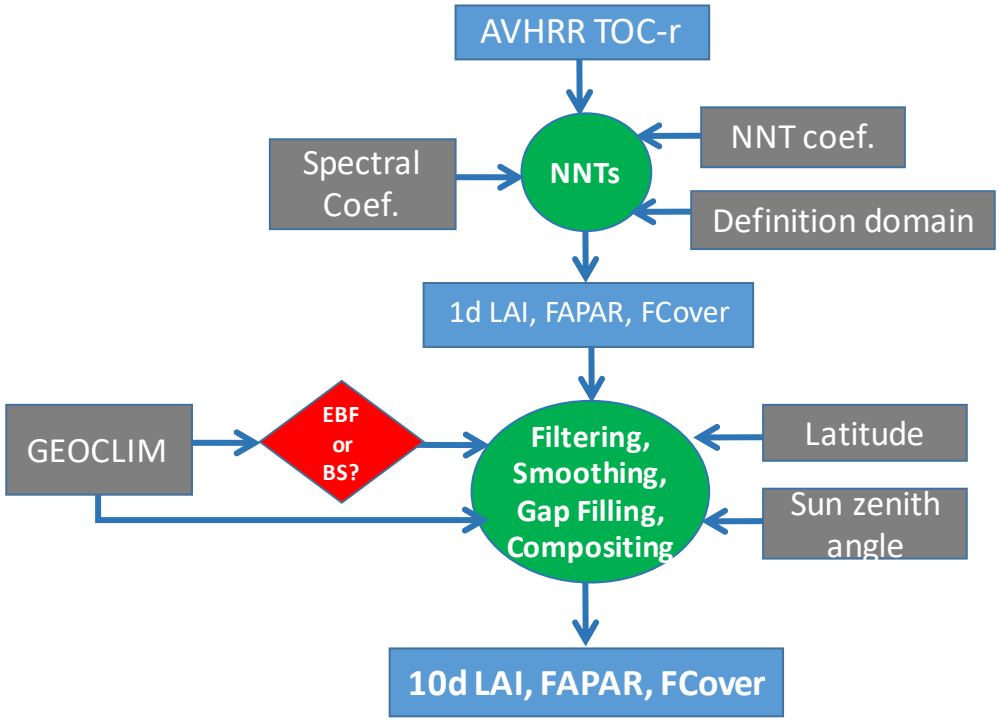

Figure 1: Flow chart the GEOV2-AVHRR retrieval algorithm. The algorithm starts from the daily LTDR AVHRR daily reflectance products. Neural networks (NNTs) are used first to derive instantaneous estimates from top of the canopy directionally normalized TOC-r reflectances in the red and near infrared spectral bands (Branch A). The output is the instantaneous first guess of the products. Then, temporal techniques are applied to generate the final GEOV2-AVHRR products at 10-day step (Branch B). The inputs of this second step are the daily estimates, the sun zenith angle of the observations, the latitude, a climatology of LAI, FAPAR and FCOVER (GEOCLIM), and the Evergreen Broadleaf Forest (EBF) and Bare Soil (BS) landcover classes derived from the climatology.

2.2.2.1 *Retrieval of instantaneous LAI, FAPAR and FCOVER estimates (Branch A)*

The Branch A is described in Figure 2. It mainly corresponds to a first estimate of instantaneous products (called here Inst. Product1).

1. ***Spectral harmonization of AVHRR reflectances (1A)***
2. ***Outlier rejection based on inputs (2A).*** AVHRR data associated with bad quality flags as well as outside the definition domain used to train the neural networks are removed. This should allow rejecting cloud/snow/water contaminated values.
3. ***Deriving daily estimates of LAI, FAPAR and FCOVER using neural networks (3A)***. The AVHRR reflectances are transformed into instantaneous products using dedicated neural networks trained over FUSED estimates from CYCLOPES and MODIS products. Inputs are the spectrally corrected AVHRR reflectance values in the red and near infrared (and the cosine of the sun zenith angle at 10h00 only for FAPAR). This will provide consistent time

series of daily products. The neural network training process was mainly consisting in the two following main steps:

a. The training database was filtered to improve the reliability of the values. This allows defining the definition domain, i.e. the region in the red and near infrared reflectance plan where valid pixels are expected to be located.
b. Training the network, i.e. adjusting network architecture and tuning the synaptic coefficients.

4. ***Outlier rejection based on output values (4A):*** outputs out of the expected physical range are discarded.

5. ***Preparation of the climatology (5A).*** Knowledge of the climatology as background information is important for the processing of the time series. A climatology was generated at the spatial resolution of AVHRR data based on GEOCLIM, a climatology of LAI, FAPAR and FCOVER derived from GEOV1/VGT time series (Annex 1).

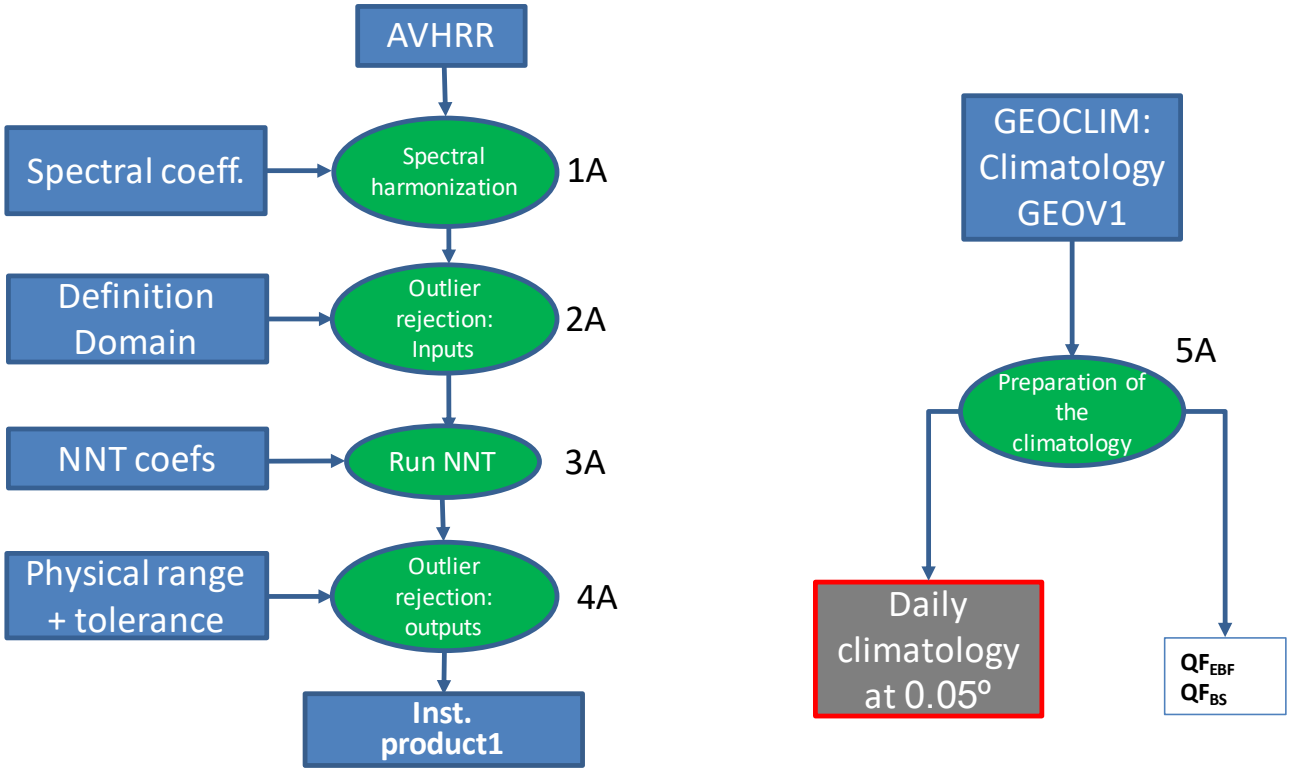

Figure 2: Flow chart describing the data preparation process (Branch A).

2.2.2.2 *Processing the time series (Branch B)*

1. ***Outlier rejection of data for EBF and high northern latitudes (1B)***.
2. ***Temporal smoothing and gap filling (2B)*** The temporal smoothing and gap filling (TSGF) method (Verger et al. 2011) is applied, i.e. a local polynomial fitting within an adaptive

window, with (large) gaps filled with the climatology values and a 2 iterations linear interpolation process.

3. ***Outlier rejection (3B)***. Data which are substantially different from the TSGF series are considered as outliers and thus rejected.
4. ***CACAO: Consistent Adjustment of the Climatology to Actual Observations (4B)***. The climatology is first decomposed into sub-seasons defined by the minimum and maximum seasonal values observed in the climatology. For each sub-season, the climatology is then adjusted to the available data allowing time shift and magnitude flexibility (Verger et al. 2013). The weighted average values are finally computed over the transition periods (where sub-seasons overlap) to get continuous and smooth products.
5. ***Generation of the GEOV2-AVHRR products using TSGF (5B)*** for each dekad with the filtered data and CACAO estimates as inputs.

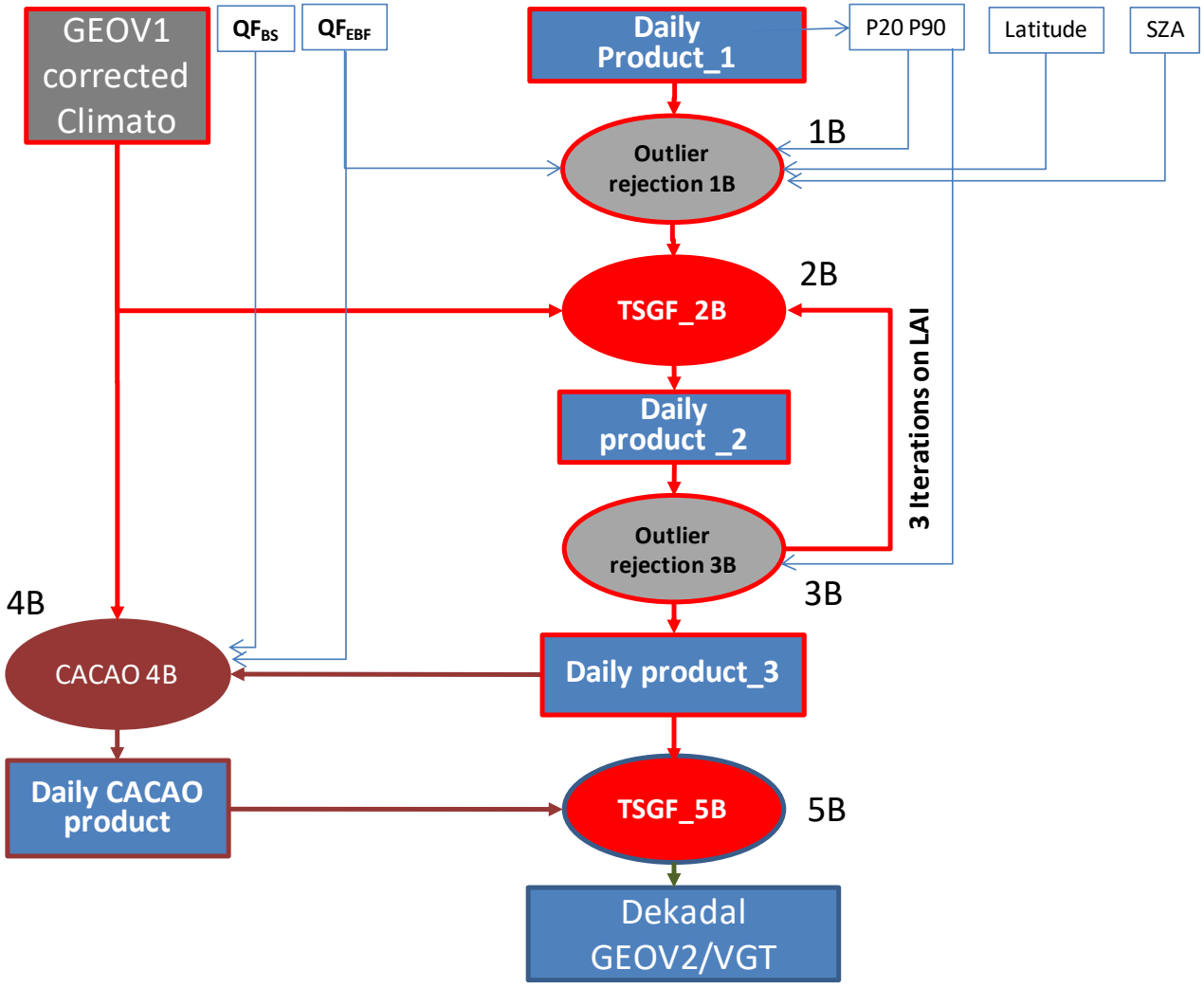

Figure 3: Flow chart describing the processing of the time series (Branch B). *Daily Product_1* is coming from step 4A, *GEOV1 corrected climatology* and quality flags QF_{EBF}/QF_{BS} come from step 5, and the sun zenith angle at 10:00 local solar time was computed in step 3A.

2.2.3 Related and previous applications

It is proposed to adapt the algorithm developed in CGLS for processing Version 2 of 1km LAI, FAPAR and FCOVER products from VEGETATION and PROBA-V data (called here GEOV2-CGLS) (Baret et al. 2014).

2.2.4 Alternative methodologies currently in use

A first version of LAI, FAPAR and FCOVER products were estimated using GEOV1-AVHRR algorithm from LTDR AVHRR version 3.0 (Baret et al. 2011).

2.2.5 Input data

In this section, the AVHR instruments and LTDR products used to retrieve the GEOV2-AVHRR biophysical products are described. Then all the inputs required for each considered pixel over the time series are presented.

2.2.5.1 *AVHRR Instrument and LTDR PRODUCTS*

The Advanced Very High Resolution Radiometer (AVHRR) sensor is an optical instrument that provides multi-spectral imaging by sensing reflected sunlight and thermal emissions.

Several AVHRR sensors have been launched since 1981 which allows getting a long time series. Table 1 gives the temporal coverage since NOAA-7.

NOAA Satellite Number	Launch date	Ascending Node	Descending Node	Service dates
7	**06/23/1981**	**1430**	**0230**	**08/19/1981-06/07/1986**
8	03/28/1983	1930	0730	05/03/1983-10/31/1985
9	**12/12/1984**	**1420**	**0220**	**02/25/1985-05/11/1994**
10	09/17/1986	1930	0730	11/17/1986-Present
11	**09/24/1988**	**1340**	**0140**	**11/08/1988-09/13/1994**
12	05/13/1991	1930	0730	05/14/1991-12/15/1994
14	**12/30/1994**	**1340**	**0140**	**12/30/1994-Present**
15	05/13/1998	1930	0730	05/13/1998-Failed
16	**09/21/2000**	**1400**	**0200**	**09/21/2000-Present**
17	06/24/2002	2200	1000	06/24/2002-Present
18	**05/20/2005**	**1400**	**0200**	**08/30/2005-Present**
19	**06/02/2009**	**2130**	**0930**	**06/02/2009-Present**

Table 1: Historic of the AVHRR temporal coverage. In bold indicates the sensors that have been actually used in this study.

The AVHRR sensor is nominally a five channel scanning sensor which images in the visible, near infrared and thermal infrared wavelength bands. Band 1 is the visible band, Band 2 is the near infrared band, and Bands 3, 4 and 5 are the thermal bands. Table 2 and Figure 4 indicate the differences of wavelength on each band for each satellite. Note that for 4 of the 7 sensors used (i.e. NOAA7, 9, 11, 14) no SWIR band is available, preventing from improved atmospheric correction.

Band Name	NOAA 7,8,9,10,11,12,14	NOAA 15,16,17,18,19	IFOV (mRad)
1 (Red)	0.58 - 0.68 µm	0.58 - 0.68 µm	1.39
2 (NIR)	0.725- 1.10 µm	0.725-1.0 µm	1.41
3A		1.58-1.64 µm	1.30

Table 2: AVHRR spectral characteristics and instantaneous field of view

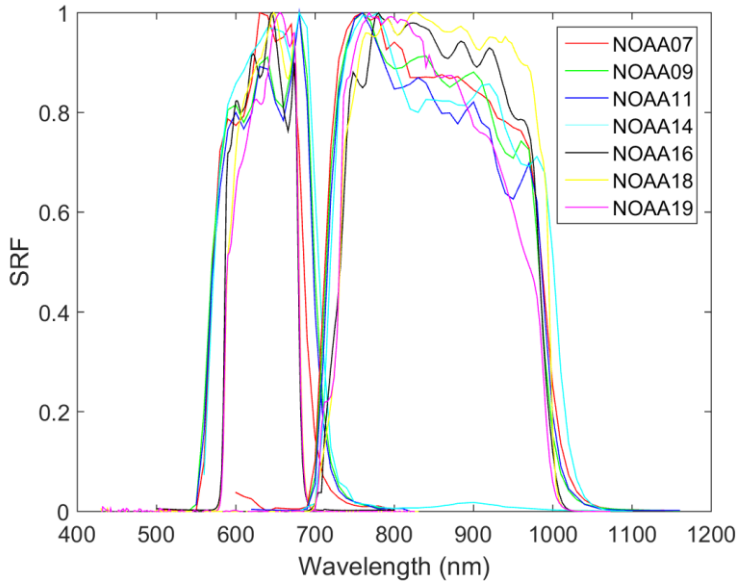

Figure 4: NOAA07 – NOAA19 spectral responses in the red and near infrared bands

The sensor has a small field of view, scanning across the Earth by the continuous 360 degree rotation of a flat scanning mirror. All the spectral channels are co-registered in order to measure energy from the same spot on the earth at the same time. The ground resolution is approximately 1.1 km at the satellite nadir from the nominal orbit altitude of about 850 km. The width of off-nadir pixels increases from 1.1 km to about 5 km at the most extreme viewing angle at the edge of the 3000 km imaging swath.

The orientation of the scan lines is perpendicular to the satellite orbit track and the speed of rotation of the scan mirror is selected so that adjacent scan lines are contiguous at the sub-satellite (nadir) position. The satellite speed and scan mirror rotation rate result in an along track pixel height of about 1.1 km. AVHRR data are broadcasted continually as well as tape-recorded onboard the

spacecraft for readout at a NOAA receiving centre. The various forms of transmission and area coverage (LAC, GAC) are explained below.

- **LAC** (Local Area Coverage) is nominally 1 km resolution AVHRR imagery recorded with the on board tape recorder for subsequent transmission during the overpass of a station controlled by NOAA. Owing to the large number of data bits, only about 11 minutes of LAC can be accommodated on a single recorder. LAC imagery can only be obtained from NOAA/NESDIS and only in their formats.
- **GAC** (Global Area Coverage) data is lower resolution (4 km) AVHRR imagery. It is derived on board the NOAA satellite by subsampling and averaging the nominal 1 km resolution AVHRR imagery. Out of every 5 normal across track LAC pixels, the 5 bands of the first four are individually averaged and all the bands of the fifth pixel are ignored. In the along track direction, only every third normal line of LAC/HRPT pixels is considered; the two intervening lines are ignored. The GAC spatial resolution is loosely said to be 4 km resolution. It provides anyway a daily global coverage which is recorded on a satellite tape recorder and then transmitted to a ground station controlled by NOAA. 115 minutes of this lower resolution imagery can be stored on a recorder, enough to cover an entire orbit of data acquisition. GAC imagery can only be obtained from NOAA/NESDIS and only in their formats.

Recently, Vermote and collaborators reanalyzed the GAC data to provide a consistent Long Term Data Record (LTDR) (Vermote and Claverie 2013; Vermote et al. 2010). The LTDR (http://ltdr.nascom.nasa.gov/ltdr/ltdr.html) provides better performances than the original GAC data due to the preprocessing improvements identified in the AVHRR Pathfinder II project and the atmospheric corrections used for MODIS.

Top of atmospheric reflectance were first calibrated using the vicarious calibration algorithm (Vermote and Kaufman 1995), cloud screening was applied using the CLAVR-1 algorithm (Stowe et al. 1999) using MODIS thresholds. Atmospheric correction was then performed using water vapor from NCEP data, ozone from TOMS data, Rayleigh scattering from NCEP atmospheric pressure simulations, and aerosols using the red (CH1).

A BRDF normalization was then achieved by applying correction parameters from POLDER in Ross-Li-Maignan model (Maignan et al. 2004). Data are provided for nadir viewing and a 45° solar zenith angle.

LTDR data are provided in hdf format at a daily temporal step and at 0.05° (5.6 km at equator) sampling interval in a latitude/longitude climate modeling grid (CMG). They are dimensioned [7200, 3600].

They correspond to a reasonable hour of ascending crossing time (close to 14:00, see Table 1). Two versions (Version 3 and version 4) for LTDR data are available. LTDR4 geometric performances were improved as compared to LTDR3 and the period has been extended to 2019 (instead of 2000 for LTDR3). Six sensors were used to cover the 1981-2019 period as described in Table 3. In order to have the longest archive with the best accuracy, we used the version 4. However, the LTDR4

dataset presents a gap lasting around almost a year (from 1st January to 2nd November 2000). On the contrary LTDR3 is available for the entire year 2000. For the year 2000, we used all available LTDR3 and LTDR4 data.

	Start Date	End Date
NOAA07	1981/06/25	1985/02/02
NOAA09	1985/01/04	1988/11/07
NOAA11	1988/11/08	1994/12/31
NOAA14	1995/01/01	2000/12/31
NOAA16	2000/11/01	2005/12/31
NOAA18	2005/07/02	2009/12/31
NOAA19	2009/06/13	2020/02/28

Table 3: Historic of the AVHRR NOAA sensors used for GEOV2-AVHRR production.

2.2.5.2 ***Inputs***

All these inputs are required for each considered pixel over the time series.

2.2.5.2.1 Top of canopy normalized reflectances

Top of canopy reflectances normalized for a standard observational configuration (zenith view angle at nadir, sun at 45° as specified in LTDR) are required as inputs. Reflectances should be expressed in terms of reflectance factor, mainly varying between 0 and 0.7 for most land surfaces outside hot-spot or specular directions and snow or ice cover. The red and near infrared AVHRR bands are used. They are provided at 0.05° resolution (≈5.6km² at the equator).

2.2.5.2.2 Sun zenith angle

Since AVHRR LTDR products are directionally normalized for nadir viewing and sun at 45° zenith angle, no information on geometry is required as input to the neural network for LAI and FCOVER. Conversely, since FAPAR is defined as the values at 10:00 local solar time, FAPAR needs the sun zenith angle (actually the cosine of the sun zenith angle is used) at that time as additional input to the neural network. The cosine of the sun zenith angle at 10:00 local solar time needs to be computed as a function of pixel latitude and day in the year (the function 'zenith' may be used for computing the sun zenith angle). On the other hand, the sun zenith angle at 10:00 local solar time will be used as an input in step 1B for filtering data at northern high latitudes.

2.2.6 Output product

The outputs are provided by application of the algorithm over each pixel at each dekadal date. They include the LAI, FAPAR and FCOVER values as described previously. The range of variation and resolution proposed are presented in Table 4. The same conventions as for GEOV2-CGLS are used here.

Variable	Physical Minimum	Physical Maximum	Max DN value	Scaling factor	Offset
LAI	0.0	7.0	210	30	0
FAPAR	0.0	0.94	235	250	0
FCOVER	0.0	1.0	250	250	0

Table 4: Minimum, maximum values and associated resolution for LAI, FAPAR and FCOVER products. Note that these values are also valid for the climatological products.

In addition to the product values, other quantitative quality indicators and quality flags are also generated (Table 5).

Variable	Physical Minimum	Physical Maximum	Max DN value	Scaling factor	Offset
Number of observations in the compositing window	0.0	60	60	1	0
Left side semi-period of compositing	0	60	60	1	0
Right side semi-period of compositing	0	60	60	1	0
RMSE with available daily observations (LAI)	0.0	7.0	210	30	0
RMSE with available daily observations (FAPAR)	0.0	0.94	235	250	0
RMSE with available daily observations (FCOVER)	0.0	1.0	250	250	0

Table 5: Minimum, maximum values and associated resolution for LAI, FAPAR and FCOVER quantitative quality indicators.

2.2.7 Methodology

The several steps of the algorithm are here presented.

2.2.7.1 *Data preparation*

2.2.7.1.1 Completing LTDR4 archive with LTDR3 data for year 2000

As already mentioned there are 10 missing months in 2000 in the LTDR4 archive. We propose to replace them by LTDR3. For the year 2000 all the available data from LTDR3 and LTDR4 will be used which will result in some overlapping of data from NOAA14 (LTDR3) and NOAA16 (LTDR4) over a period of two months. To check the validity of this approach we applied the trained neural networks to LTDR3 data over the common period (1981-1999). We compared the corresponding LAI products and found a very good relationship well centered around the 1/1 line with no bias. The observed noise reflects the different changes performed on the reflectance retrieval.

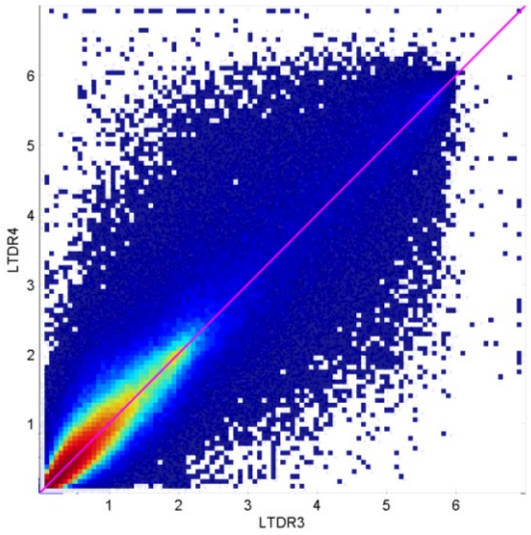

Figure 5. Scatter plot between LAI retrieved from LTDR3 and LTDR4 using the same neural network.

2.2.7.1.2 GEOCLIM: climatology of GEOV1/VGT LAI, FAPAR and FCOVER

GEOCLIM (Verger et al. 2015), a climatology of LAI, FAPAR and FCOVER defined as the average inter-annual value from GEOV1/VGT time series, is used as background information for the temporal processing in Branch B. Based on the LAI climatology, pixels corresponding to evergreen broadleaf forest (EBF) and permanent bare soils (BS) were identified by a particular quality flag (QF). This work is described in Annex 1.

For the pixels identified as EBF, the corresponding flag QC(11) in Table 9 is set to 1. For the pixels identified as BS, the flag QC(12) in Table 9 is set to 1.

2.2.7.1.3 Calibration of neural networks

A neural network (NNT) for each of the 3 variables considered (LAI, FAPAR, and FCOVER) was calibrated as described in Annex 2.

2.2.7.2 *Retrieval of instantaneous LAI, FAPAR and FCOVER estimates (Branch A)*

2.2.7.2.1 Spectral harmonization (Step 1A)

We applied a spectral harmonization to correct the slight differences in the spectral responses of several AVHRR NOAA sensors in the red and NIR bands (Figure 4). A relative correction with the NDVI (Trishchenko et al. 2002) is applied for each band *i* to estimate NOAA-16 like reflectances, ρ_{16}^{i}, from the reflectance value measured by the other NOAA-xx sensors, ρ_{xx}^{i}:

$$\rho_{16}^{i} = \rho_{xx}^{i} + \rho_{xx}^{i} * (a_{xx}^{i} * NDVI_{xx}^{3} + b_{xx}^{i} * NDVI_{xx}^{2} + c_{xx}^{i} * NDVI_{xx})$$

The correction coefficients (a_{xx}^{i}, b_{xx}^{i}, c_{xx}^{i}; Table 6) were fitted on simulations based on the PROSAIL radiative transfer model (Jacquemoud et al. 2009), using the specific spectral response functions of the several NOAA-xx sensors (Figure 4).

	RED			NIR		
	c3	c2	c1	c3	c2	c1
NOAA7	-0.472356828	0.320957648	-0.083407272	0.061470757	-0.05292409	0.034249109
NOAA9	-0.415363608	0.183403764	-0.085707595	0.091997568	-0.120327789	0.07633715
NOAA11	-0.638173822	0.438275038	-0.158994859	0.106433007	-0.143932073	0.088786746
NOAA14	-0.671403652	0.466115322	-0.194386392	0.05249465	-0.035273029	0.017968874
NOAA16	0	0	0	0	0	0
NOAA18	0.252741652	-0.185588803	0.032741312	-0.015916103	0.046098269	-0.03101059
NOAA19	0.247196889	-0.14302899	0.013464287	0.035956883	-0.08920432	0.060300707

Table 6: Spectral conversion coefficients between the several AVHRR NOAA sensors.

2.2.7.2.2 First outlier rejection: input out of range (Step 2A)

Checking the validity of the AVHRR inputs

The AVHRR data validity must be first checked and all the data having bits 14, 9,8,4,2,1 equals to 1 must be discarded.

Bit Number	Description	Meaning
15	Polar flag: latitude > 60° (land) or > 50° (ocean)	1 = yes, 0 = no
14	BRDF-correction issues	1 = yes, 0 = no
13	RHO3 value is invalid	1 = yes, 0 = no
12	Channel 5 value is invalid	1 = yes, 0 = no
11	Channel 4 value is invalid	1 = yes, 0 = no
10	Channel 3 value is invalid	1 = yes, 0 = no
9	Channel 2 value is invalid	1 = yes, 0 = no
8	Channel 1 value is invalid	1 = yes, 0 = no
7	Channel 1-5 are invalid	NA
6	Pixel is at night (high solar zenith angle)	1 = yes, 0 = no
5	Pixel is over dense dark vegetation	1 = yes, 0 = no
4	Pixel is over sun glint	1 = yes, 0 = no
3	Pixel is over water	1 = yes, 0 = no
2	Pixel contains cloud shadow	1 = yes, 0 = no
1	Pixel is cloudy	1 = yes, 0 = no
0	Unused	NA

Table 7: Quality flags associated to LTDR4 AVHRR data

Applying the definition domain over the inputs

The AVHRR data that are outside the definition domain (Annex 2) are first rejected.

$$\begin{cases} if\ NIR \geq RED \\ if\ NIR \leq -2.41x^3 + 4.32x^2 - 1.16x + 0.54\ and\ RED < 0.685\ , P_{step1A} = P_{step1A}, \\ if\ NIR \leq 1\ and\ \ RED \geq 0.685 \end{cases} \quad [1]$$

$$else\ P_{step1A} = invalid\ value$$

2.2.7.2.3 Deriving instantaneous estimates of LAI, FAPAR and FCOVER using neural networks (Step 3A)

A neural network (NNT) was previously calibrated for each of the 3 variables considered (LAI, FAPAR, and FCOVER) (see Annex 2). They are then applied to each individual AVHRR observation (one pixel at a given date).

The inputs of the neural networks are:

- For LAI and FCOVER, LTDRV4 surface reflectance in the red and near infrared bands. No sun zenith angle needs to be added since the LTDR are normalized at nadir viewing for 45° sun zenith angle. Note that for year 2000 (January to October), LTDRV3 are used.

- For FAPAR, LTDRV4 surface reflectance in the red and near infrared bands, as well as the cosine of the sun zenith angle at 10:00 solar time to be consistent with GEOV2-CGLS FAPAR definition, i.e. black-sky FAPAR at 10:00 solar time.

The outputs the corresponding instantaneous LAI, FAPAR and FCover values.

2.2.7.2.4 Outlier rejection: output out of range (Step 4A)

P_{step3A} values that are outside the physical range of variation of the variables extended by the tolerance limits (Table 8) are also rejected. Values that are within the tolerance limits (Table 8) but higher (lower) than the physical maximum P_{max} (minimum, P_{min}) (Table 4) are fixed to the physical maximum (minimum).

$$\begin{cases} if\ P_{step2A} < P_{min}^{tol}, P_{step3A} = invalid\ value \\ if\ P_{step2A} > P_{max}^{tol},\ P_{step3A} = invalid\ value \end{cases} \quad [9]$$

$$\begin{cases} if\ P_{min}^{tol} \leq P_{step2A} < 0,\ P_{step3A} = 0 \\ if\ P_{max} < P_{step2A} \leq P_{max}^{tol}, P_{step3A} = P_{max} \end{cases}$$

$$else\ P_{step3A} = P_{step2A}$$

	LAI	FAPAR	FCOVER
P^{tol}_{min}	-0.20	-0.05	-0.05
P^{tol}_{max}	10.0	0.99	1.05

Table 8: Tolerance limits (Minimum (P^{tol}_{min}) and maximum (P^{tol}_{max})) used for the rejecting output outside the expected physical range of variation.

2.2.7.2.5 Preparation of the LAI, FAPAR and FCOVER climatology (Step 5A)

The GEOCLIM (Verger et al. 2015) product, a global climatology of LAI, FAPAR, and FCOVER from GEOV1/VGT products for 1999–2010 and the quality flags identifying EBF and bare soil areas (Annex 1: GEOCLIM, a climatology of GEOV1 LAI, FAPAR and FCOVER) are used as an input of the GEOV2 algorithm. Some preparatory steps of spatial and temporal resampling are required to ingest the GEOCLIM climatology in the GEV2-AVHRR processing chain:

2.2.7.2.5.1 Resampling the corrected climatology to the AVHRR spatial resolution

The GEOCLIM climatology at the original 1/112º spatial resolution of VGT was subsequently resampled at 0.05º to match AVHRR products. Since both VGT and AVHRR products are on a Plate-Carrée grid, a simple aggregation of the 5x5 VGT pixels centered around the AVHRR one is performed. Similarly, the EBF and BS quality flags (QF) were degraded at 0.05 resolution by

assigning the dominant QF in the 5x5 window. The global corrected climatology as well as the associated BS and EBF quality flags at 0.05º has been generated by CREAF and provided to CNES as an input of the processing chain.

2.2.7.2.5.2 Interpolation at the daily time step over the entire period

The 36 dekadal climatology is repeated for all the years of the time series extended by 1 year on each side to prevent border effects. This climatology is finally interpolated at the daily time step for further use as background information for gap filling in branch B.

2.2.7.3 ***Processing the time series (Branch B)***

2.2.7.3.1 Computation of P20 and P90 for LAI

P20 is defined as the 20-percentile of AVHRR LAI estimates (Daily Product_1) computed over the whole time series.

P90 is defined as the 90-percentile of AVHRR LAI estimates (Daily Product_1).

P20 and P90 are subsequently used in step 1B and 3B.

2.2.7.3.2 Outlier rejection (Step 1B)

For this outlier rejection, emphasis was put on LAI products that show the highest sensitivity to possible problems in reflectance values. Therefore, when an outlier is detected on LAI data, it is also considered as an outlier for FAPAR and FCOVER to keep a high level of consistency between the three variables. We filtered the noisy data based on expert knowledge of the expected seasonality:

- For the high northern latitude (latitude>55º), the LAI (FAPAR, FCOVER) values in winter time (SZA>70º where SZA is the sun zenith angle at 10:00 solar time as computed in the step 1B for computing the FAPAR) are expected to be relatively stable and low due to the low temperatures, short days, and low illumination during winter at these high latitudes. However observations are affected by snow cover or very poor illumination conditions that introduce a positive bias in the LAI estimates. For the pixels at latitude>55º with P90>0.5, the LAI values > P20 and 0.5 in winter time, SZA>70º, were considered as outliers and rejected.
- For pixels identified as EBF (QF_EBF=1), a minimum seasonality and high values of LAI were assumed. The observed artifacts in EBFs are mostly associated to the high cloud cover observed in the Equatorial and tropical latitudes which introduce a negative bias in LAI. The LAI values < 5.5 and P90, i.e. the 90-percentile of AVHRR LAI estimates (Daily Product_1), were rejected.

$$\begin{cases} if\ latitude > 55º\ and\ P90 > 0.5\ and\ SZA > 70°\ and\ LAI > P20\ and\ LAI > 0.5,\ P_{step1B} = invalid\ value \\ if\ QF_{EBF} = 1\ and\ LAI < P90\ and\ LAI < 5.5,\ P_{step1B} = invalid\ value \end{cases}$$

$$else\ P_{step1B} = P_{step3A} \qquad [10]$$

2.2.7.3.3 Temporal smoothing and gap filling (TSGF) (Step 2B)

The daily products after the first outlier rejection were smoothed and gap filled using the same techniques (Verger et al. 2011) as the ones considered for processing the climatology (step 5A). This is achieved similarly at the dekadal time step with however some particularities that account for the important noise associated to the raw data (Figure 6):

- ***Adjusting the length of the compositing window to get 6 observations on each side of the dekadal date.*** After evaluating several widely used temporal filters, a simple but robust method based on the adaptive Savitzky-Golay (SG) filter (Savitzky and Golay, 1964; Chen et al., 2004) was selected to smooth the data. The fixed and symmetric smoothing compositing window of the standard SG polynomial fitting method was replaced by an adaptive process with variable length and asymmetric (in time) compositing window. The number of observations within each side of the dekadal date being smoothed was fixed to 6 instead of 3 as previously considered for the climatology. This difference is explained by the more smooth climatology values as compared to the daily estimates. The length of the window is therefore variable, depending on the available observations in the vicinity of the dekadal date considered. However, a maximum ±60-days compositing window was used to allow adaptation to the local variations in the data. Further, a minimum ±15-days period was imposed even if more than 6 observations exist within each semi-period since it increases the robustness of the fitting.
- ***Use of the climatology to fill missing values.*** If the number of available observations in the maximum 60-days semi-compositing window is lower than 6 observations, available observations are systematically completed with 6 climatology values located every 10 days evenly distributed over the 60 days period. If there are no climatology values, this will result in a missing value at the considered dekadal date. The considered climatology for filling gaps is a daily climatology that results from the linear interpolation of the original dekadal climatology as described in step 5A.
- ***Fit polynomial model.*** A weighted polynomial fitting is applied with weighting factors, *W*, computed according to the distance of the daily estimates to the TSGF outputs derived from the previous iteration. A sigmoidal function was considered for computing the weights W with less weight associated to the values smaller than the previous TSGF estimates since the low values have more chances to be contaminated by residual clouds or snow.

  $$W = 2/(1 + \exp(-2 * \delta)) \quad [11]$$

  Where δ is the difference between the daily estimates and the TSGF outputs. To put less emphasis on the climatology values used to fill gaps, weights of the climatology fill values were multiplied by a factor of 0.5. For the first iteration of TSGF, weights of actual data were fixed to 1 and to 0.5 for the climatology.
- ***Use interpolation to fill values.*** Finally, to fill the residual gaps, a linear interpolation within a ±60-days window is applied. A simple linear interpolation based on a local moving window of ±60-days length was applied to fill gaps in the time series. To improve the efficiency of gap

filling, an iterative process (*niter*=2 iterations) was considered: the gain of available data achieved with the first iteration allows improving robustness and continuity in the gap-filled data through a second iteration. Gaps longer than 120 days are not filled and will result in missing data.

- Finally to avoid possible artifacts introduced by divergences of the temporal filters being applied, the TSGF values were forced to the physical range of variation of the LAI, FAPAR and FCOVER (Table 4).

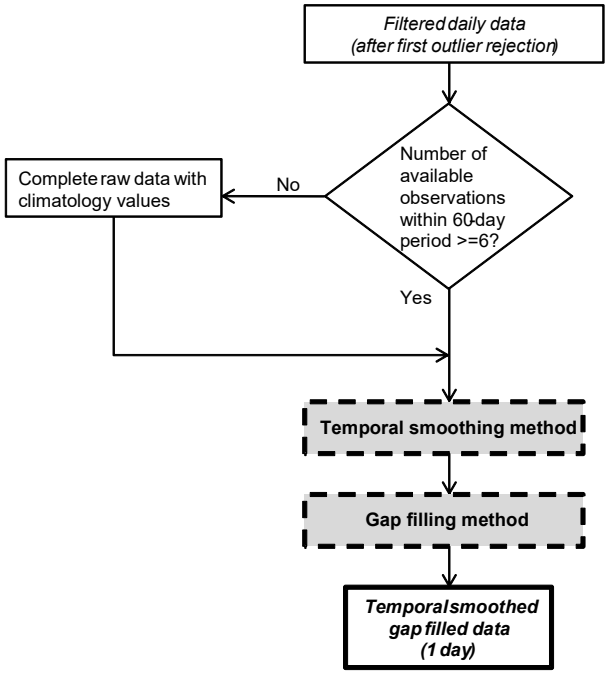

Figure 6: Flow chart showing how the temporal smoothing gap filling (TSGF) algorithm works.

2.2.7.3.4 Outlier rejection (Step 3B)

Similarly to the previous outlier rejection (step 1B), emphasis was put on LAI product for identifying outliers. The original data were filtered by comparison between LAI values and the temporal smoothed and gap filled (TSGF) LAI series. A point under (respectively over) the TSGF estimates (interpolated at daily step from the dekadal values) was considered as an outlier if its absolute distance to all the TSGF LAI values within a ±5-day window is either:

- greater than 0.10 and the 15% of the TSGF value.
- lower than 0.10 and the 15% of the TSGF value.

Considering a ±5-day window prevents from eliminating too many observations during periods of high rate of variation of LAI.

The process is repeated *niter* times, *niter* being the number of iterations used for TSGF (*niter* was fixed to 3). To avoid rejecting false outliers the upper values were only filtered in the last iteration. The more restrictive criteria imposed here to the values under TSGF upper envelope accounts for the effect of residual clouds that are systematically lower than the actual value of the LAI estimates (Figure 7). Similarly to prevent rejecting too many low values in the base level due to a possible

limitation of TSGF to fit the data in these regions, a higher negative distance of 0.5 to TSGF is considered for the values within ±0.5 of the base level. The base level is defined as the maximum of percentile 20 of the data (P20) and a threshold fixed to 0.5 LAI. This last condition to avoid removing valid data in the base level is only applied when the percentile 90 of the data is higher than 0.5. The performance of this automatic method is illustrated in Figure 7.

For the LAI values lower than the TSGF upper envelope, the following conditions are applied to filter outliers in the *niter* iterations:

$$\text{If} \begin{Bmatrix} LAI_t < TSGF_t \\ \min\left(\left|LAI_t - \left(\overrightarrow{TSGF_{t-5,t-4\ldots t+5}}\right)\right|\right) > \max(0.1, 0.15 * TSGF_t) \end{Bmatrix}, P_{step3B} = invalid\ value$$

$$elseif \begin{Bmatrix} LAI_t < TSGF_t \\ \min\left(\left|LAI_t - \left(\overrightarrow{TSGF_{t-5,t-4\ldots t+5}}\right)\right|\right) > \max(0.1, 0.15 * TSGF_t) \\ P90 > 0.5 \\ |LAI_t - \max(P20, 0.5)| < 0.5 \\ |LAI_t - TSGF_t| < 0.5 \end{Bmatrix}, P_{step3B} = P_{step2B} \quad [12]$$

$$else, \qquad P_{step3B} = P_{step2B}$$

For the LAI values higher than TSGF, the following conditions are applied to filter outliers in the last iteration:

$$\text{If} \begin{Bmatrix} LAI_t > TSGF_t \\ \min\left(\left|LAI_t - \left(\overrightarrow{TSGF_{t-5,t-4\ldots t+5}}\right)\right|\right) > \max(0.1, 0.15 * TSGF_t) \end{Bmatrix}, P_{step3B} = invalid\ value \quad [13]$$

$$else, \qquad P_{step3B} = P_{step2B}$$

For FAPAR and FCOVER variables and pixels identified as EBF, the step 3B is not applied.

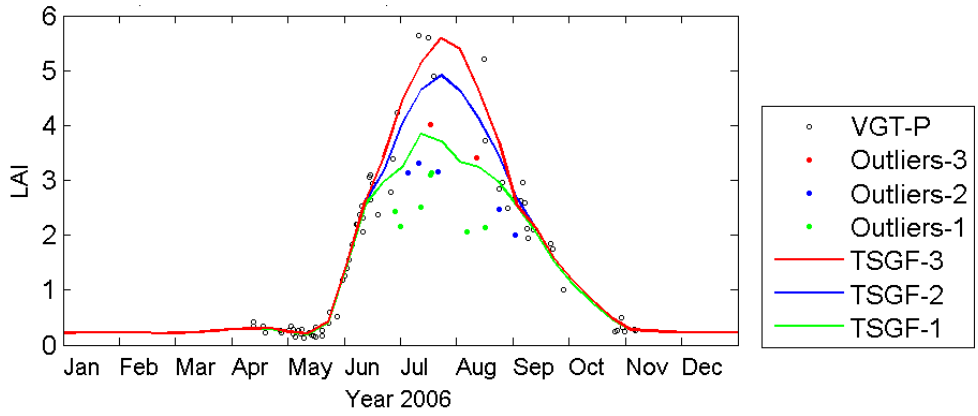

Figure 7: Illustration of the 3-iterations of TSGF filtering (continuous line) to eliminate contaminated data (filled circles). Empty circles correspond to valid data.

2.2.7.3.5 Subsequent iterations of the steps 2B and 3B

Because the TSGF should rely mostly on valid observations, the step 2B was repeated after the outlier rejection performed in step 3B which requires itself a first application of TSGF. To deal with the significant noise in the data this process is conducted iteratively. A total number of niter=3 iterations is proposed for LAI. Figure 7 illustrates improvements in TSGF outputs through the proposed iterative process. For FAPAR and FCOVER variables the iterative application of steps 2B and 3B is not required since outliers were previously filtered focusing on LAI as described previously. Similarly, for pixels identified as EBF these iterations are not necessary. For FAPAR, FCOVER step 2B are only applied once and step 3B is not applied. For EBFs steps 2B and 3B are not applied.

2.2.7.3.6 Consistent Adjustment of the climatology to actual observations (CACAO, Step 4B)

Adjusting climatological patterns to actual observations was shown to efficiently capture the product dynamics and the inter-annual anomalies while filling gaps and smoothing biophysical products in a robust way (Baret et al. 2011; Verger et al. 2013). CACAO consists in fitting the climatology to the actual daily products by shifting and scaling the climatology values over portions of the seasonal cycle (sub-seasons) (Figure 8). The CACAO process is applied to each sub-season and will result in estimates at the daily time step. A sub-season is defined by the period between two consecutive extrema in the climatology. The following steps were thus followed:

- ***Decompositing the climatology into sub-seasons.*** The global extrema (minima and maxima) points from the climatology time series should be identified first. However, to exclude possible false extrema in the time series due to the effect of residual noise in the signal, extrema values that differ by less than 0.10 LAI (0.025 for FAPAR and FCOVER) or the 15% of the median value of the climatology were excluded. The sub-seasons were slightly extended by considering the minimum extra time window before and after the period containing either 30% of the signal dynamics or 30% of the period length (in days) of the adjacency sub-

seasons. This allowed more robust fit by providing clearer temporal features on which the adjustment could grasp.

- ***Shifting and scaling the climatology for each sub-season.*** The climatology was fitted to the actual daily observations for each year and each sub-season. The daily climatology P^{clim} was fitted to the daily P data by considering a scale factor, scale, and a temporal shift, $shift$:

$$\hat{P}(t) = scale \cdot P^{clim}(t + shift) \quad [14]$$

If $\hat{P}$ follows the usual climatological pattern, P^{clim}, $scale = 1$ and $shift = 0$. The two parameters $(scale, shift)$ are found by minimizing the cost function defined by the RMSE between daily observations and the estimated product values after fitting the climatology.

The shift parameter was allowed to vary between $-60 < shift < 60$ by steps of 5 days which resulted in 25 adjustments between the shifted climatology and the P data. A minimum of 10% of the potential observations representing 30% of the signal in the sub-season are required for fitting the climatology. Otherwise, the original climatology is considered as a backup solution. For pixels identified as bare soil or EBF with almost no seasonality, the climatology is adjusted over the whole time series if a minimum of $n = 10$ observations exist.

In the transition between sub-seasons, a weighted average between $\hat{P}$ estimates from the two sub-seasons was considered as the final solution. A linear weight contribution varying between 1 and 0 (between 0 and 1) was assigned to the first (second) sub-season estimates in the overlapping period.

- Finally to avoid possible artifacts introduced by divergences of the temporal filters being applied, the CACAO values were forced to the physical range of variation of LAI, FAPAR and FCOVER (Table 4).

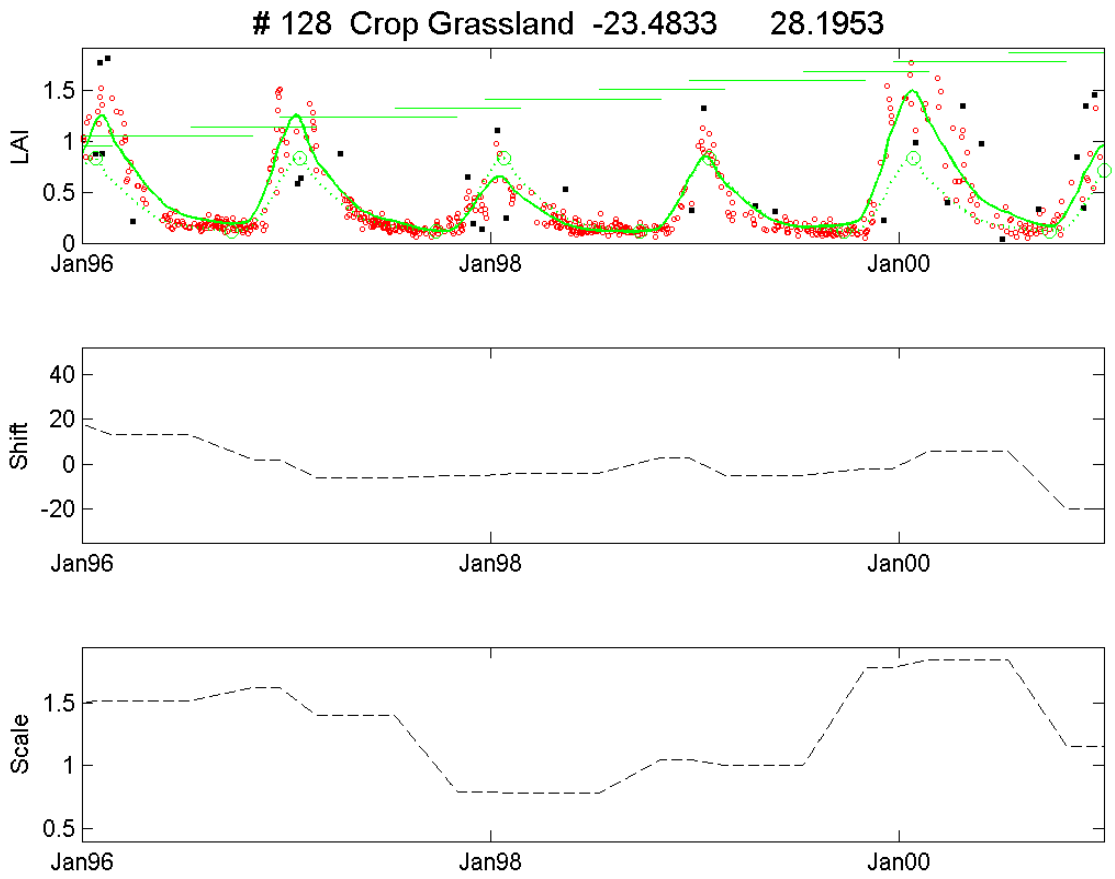

Figure 8: Illustration of CACAO method. Top: the dotted green line corresponds to the original climatology, the green circles indicate the position of the extrema in the climatology, the green segments indicate the duration of the sub-seasons, the continuous line corresponds to the fitted climatology: CACAO, red circles correspond to the data and black squares are outliers. Middle: shift factor (day units) representing the temporal anomalies of LAI data as compared to the climatological pattern. Bottom: Scale factor (LAI units) representing the magnitude anomalies of LAI.

2.2.7.3.7 Computation of the dekadal GEOV2 product (Step 5B)

TSGF was finally applied over the filtered daily observations at each dekadal step for generating the final GEOV2 product. Six observations within a maximum period of 60 days on each side of the dekadal dates are necessary. However, the minimum period considered is 30 days instead of 15 days as in step 2B. The minimum period was extended in step 5B to improve the smoothness of the resulting temporal profile. Further, the CACAO product was used to fill gaps in the time series in place of the standard climatology as it was used previously in the step 2B. Since CACAO is expected to be closer to the data as compared to the original climatology, the use of CACAO helps in the estimation of the final product over period with missing observations.

2.3 QUALITY INDICATORS

2.3.1 Quality flags

The quality flag associated to the GEOV2-AVHRR products is coded in 16bit as described in Table 9. It is consistent with the one used for GEOV2-CGLS products.

	Bit = 0	Bit = 1
0	Unused	
1 : Processing	The pixel is processed (land)	The pixel is unprocessed (water)
2 : Climatology status	OK	Missing climatology
3 : Filling	No filling procedure	The number of valid observations at least on one side of the ±60-day period is lower than 6 and a gap filling procedure (Bit 13-14) is applied
4	Reserved	
5	Reserved	
6 : Input status	At least one valid data within ±60 days	No valid data within ±60 days
7 : LAI status	OK	Out of range or invalid
8 : FAPAR status	OK	Out of range or invalid
9 : FCOVER status	OK	Out of range or invalid
10 : SZA status	SZA <= 70º or latitude <= 55º	SZA > 70º and latitude > 55º
11 : EBF status	Pixel is not recognized as Evergreen Broadleaf Forest	Pixel is recognized as Evergreen Broadleaf Forest
12 : BS status	Pixel is not recognized as Bare Soil	Pixel is recognized as Bare Soil
13 : Climatology filled	Not filled	Filled with climatology
14 : Gap filled	Not filled	Filled with interpolation
15	Unused	

Table 9: Description of the quality flag provided for the LAI, FAPAR, FCOVER.

2.3.2 Computation of the associated quality assessment

The following quality indicators associated to the GEOV2-AVHRR products are proposed:

- The number of valid AVHRR observations, *NOBS*, in the composition period that are used to compute the product value (Step 5B). The more observations, the more reliable are the products.
- The length in days of each semi-period (before and after the dekadal date) of composition. The shorter the semi-periods, the more reliable are the products.
- The RMSE of the final decadal product, $P^{GEOV2/AVHRR}(d)$, as compared to the instantaneous estimates, $P(i)$, in the compositing period.

$$RMSE(d) = \sqrt{\frac{\sum_i^{NOBS}(P^{GEOV2/AVHRR}(d) - P\quad(i))^2}{NOBS}} \qquad [15]$$

The RMSE is computed only if $NOBS \geq 2$, otherwise it is set as a missing value.

3 LIMITATIONS

GEOV2-AVHRR capitalizes on the development and validation of already existing products: CYCLOPES version 3.1 and MODIS collection 5 and the use of neural networks. The CYCLOPES and MODIS products used in the training dataset, the efficacy of the training process and the criteria used to define the input outliers will determine, respectively, the magnitude and range of variation of the final products, their reliability and the definition domain used to remove contaminated values.

The final product is also dependent on the criteria used to filter the output outliers, particularly for the tropical forests and high latitudes. Outlier rejection constitutes a critical step in the algorithm. The efficiency of the temporal methods used in the composition of products from daily estimates depends on the level of noise and gaps in the time series and on the reliability of the auxiliary data (climatology) used as a background information to fill gaps.

The main identified limitations are associated to the input data:

- The temporal consistency of long time series of GEOV2-AVHRR products depends mainly on the temporal consistency of input TOC reflectances between the different AVHRR NOAA sensors used for the generation of 1981-2019 LTDR dataset. A spectral harmonization was here applied to correct the differences in the spectral response function of the sensors.
- Significant efforts were performed in LTDR to reprocessed AVHRR NOAA reflectances and V4 (used as input in GEOV2-AVHRR) appears to constitute an improvement as compared to V3 (used in GEOV1/AVHRR) in terms of the number of data being delivered. The period was extended from the year 2000 to 2019. Nevertheless, residual problems persist in LTDRV4 mainly at very high latitudes and near the Equator mainly due to atmospheric effects and cloud contamination. The relatively broad red (0.58 - 0.68 µm) and near infrared (0.725 - 1.10 µm) bands on the AVHRR increase the sensitive to atmospheric conditions (Vermote et al. 2009). An important limitation of LTDRV4 dataset in terms of continuity is that the data is missing for the most part of the year 2000. This is not the case for the previous version LTDRv3 data. For this reason we used LTDRv3 to complete LTDRv4 data for the year 2000. A new version, Version 5 of LDTR is now available but not at the moment of the generation of GEOV2-AVHRR.
- The climatology plays an important role for gap filling and temporal smoothing of the data. Possible artifacts in the climatology are translated to the final products. When the climatology is missing no auxiliary information is available to fill gaps in GEOV2 time series. The GEOCLIM climatology (Verger et al. 2015) based on GEOV1-VGT time series, corrected from artifacts and resample to AVHRR spatial resolution was used since no GEOV2 climatology was available at the time the study was conducted.
- Similarly, the quality flags used for the identification of bare soil (BS) and evergreen broadleaf forests (EBF) were generated based on GEOCLIM climatology (Verger et al. 2015). The same quality flags were used in GEOV2-AVHRR and GEOV2-CGLS processing in order to achieve consistency in the time series.

- The approach used to process pixels flagged as evergreen broadleaf forest (EBF, QC(11)=1 in Table 9) constitutes an oversimplification of the reality because of the possible seasonality of EBFs. The high uncertainty associated with the data due to poor atmospheric correction and very high cloud occurrence in equatorial and tropical latitudes prevented the extraction of meaningful phenology at the resolution of the individual pixels of 1 km. The high spatial and temporal resolution of Sentinel2 sensors should improve the monitoring of vegetation in these problematic areas.
- In cases of a wrong identification of a pixel as an EBF, GEOV2 only reproduces the high values but not the actual seasonality of the pixel.
- The algorithm uses a static mask for EBF based on the climatology for the period 1999-2010. Consequently, for pixels flagged as EBF, the GEOV2 product may not capture deforestation processes. This mask may require to be updated in the future.
- The values of LAI, FAPAR and FCover over pixels identified as BS (QC(12)=1 in Table 9) are close to zero but not strictly zero. Some users may prefer forcing the values of biophysical variables to zero for pixels flagged as BS.
- GEOV2-AVHRR LAI, FAPAR and FCover variables are retrieved over inland waters not discriminated as water in the land/sea mask (QC(1)=0 in Table 9). Inland water pixels are mostly identified as Bare Soil (BS, QC(12)=1 in Table 9) based on GEOCLIM climatology. Although it would bring an improvement to mask the inland waters, it does not exist inland water mask reliable enough to be used without taking the risk to create side effects in the products.

The user should use the product with due attention to the quality flags values as well as the associated uncertainties, in particular for areas with long periods of cloudiness.

4 CONCLUSION

The GEOV2-AVHRR, LAI, FAPAR and FCOVER products capitalize on the efforts undertaken to pre-process the AVHRR temporal series, resulting in the LTDR data, and the recent development of improved processing of products resulting in the GEOV2-CGLS dataset. The GEOV2-AVHRR time series were designed to provide smooth and continuous time series. Emphasis was therefore put on the outlier rejection, smoothing and gap filling of the daily products. In order to achieve consistency with GEOV2-CGLS products we used the same algorithm with some adaptations to the characteristics of LTDR data.

A dedicated validation exercise is achieved in [THEIA-RP-44-0281-CREAF] following the guidelines proposed by the CEOS/LPV. The performances of GEOV2-AVHRR were quantified with regards of GEOV2-CGLS and other existing products as well as compared to ground data. Validation results showed very good agreement with the GEOV2-CGLS products.

The user should use the product with due attention to the QF values as well as proxy of uncertainties coming mainly from the RMSE values and the number of actual observations used.

The combination of the GEOV2-AVHRR time series (1981-2019) with GEOV2-CGLS time series *(*1999 - present*)* results in the longest consistent time series of LAI, FAPAR and FCOVER. Because AVHRR sensors are still in orbit, the coming years will be processed as soon as the corresponding LTDR data will be available. This will ensure the expansion of the GEOV2-AVHRR time series after 2019. The CGLS Sentinel-3 products based on the same principles also ensures continuity of the time series.

5 REFERENCES

Baret, F., Leroy, M., Roujean, J.L., Knorr, W., Lambin, E., & Linderman, M. (2003). CYCLOPES User Requirement Document. In. Avignon: INRA-CSE

Baret , F., Verger, A., & Weiss, M. (2014). Algorithm Theorethical Basis Document Leaf Area Index (LAI), Fraction of Absorbed Photosynthetically Active Radiation (FAPAR) and Fraction of green Vegetation Cover (FCover). Version 2.0 (GEOV2). In (p. 71). Avignon: INRA-EMMAH

Baret , F., Weiss, M., & Kandasamy, S. (2010). Climatology of LAI, FAPAR and FCOVER products (V1). In (p. 30). Avignon (France): INRA-EMMAH

Baret, F., Weiss, M., Verger, A., & Kandasamy, S. (2011). BioPar Methods Compendium - LAI, FAPAR and FCOVER from LTDR AVHRR series. In, *Report for geoland2 EC contract FP-7-218795. Available at* http://www.geoland2.eu/portal/documents/CA80C881.html (p. 46). Avignon: INRA-EMMAH

Chen, J.M., Menges, C.H., & Leblanc, S.G. (2005). Global mapping of foliage clumping index using multi-angular satellite data. *Remote Sensing of Environment, 97*, 447-457

Defourny, P., Bicheron, P., Brockmann, C., Bontemps, S., Van Bogaert, E., Vancutsem, C., Pekel, J.F., Huc, M., Henry, C., Ranera, F., Achard, F., di Gregorio, A., Herold, M., Leroy, M., & Arino, O. (2009). The first 300 m global land cover map for 2005 using ENVISAT MERIS time series: a product of the GlobCover system,. In, *Proceedings of the 33rd International Symposium on Remote Sensing of Environment*. Stresa (Italy)

Garrigues, S., Allard, D., Baret, F., & Weiss, M. (2006). Influence landscape spatial heterogeneity on the non-linear estimation of leaf area index from moderate spatial resolution remote sensing data. *Remote Sensing of Enviroment, 105*, 286-298

Jacquemoud, S., Verhoef, W., Baret, F., Bacour, C., Zarco-Tejada, P.J., Asner, G.P., François, C., & Ustin, S.L. (2009). PROSPECT + SAIL models: A review of use for vegetation characterization. *Remote Sensing of Environment, 113*, S56-S66

Maignan, F., Bréon, F.M., & Lacaze, R. (2004). Bidirectional reflectance of Earth targets: evaluation of analytical models using large set of spaceborne measurements with emphasis on the hot-spot. *Remote Sensing of Enviroment, 90*, 210-220

Prince, S.D. (1991). A model of regional primary production for use with coarse resolution satellite data. *International Journal of Remote Sensing*

Roujean, J.L., Leroy, M., & Deschamps, P.Y. (1992). A bidirectional reflectance model of the Earth's surface for the correction of remote sensing data. *Journal of geophysical research, 97*, 20455-20468

Stowe, L.L., Davis, P.A., & McClain, E.P. (1999). Scientific basis and initial evaluation of the CLAVR-1 global clear/cloud classification algorithm for the advanced very high resolution radiometer. *Journal of Atmospheric and Oceanic Technology, 16*, 656-681

Trishchenko, A.P., Cihlar, J., & Li, Z. (2002). Effects of spectral response function on surface reflectance and NDVI measured with moderate resolution satellite sensors. *Remote Sensing of Environment, 81*, 1-18

Verger, A., Baret, F., & Weiss, M. (2011). A multisensor fusion approach to improve LAI time series. *Remote Sensing of Enviroment, 115*, 2460-2470

Verger, A., Baret , F., & Weiss, M. (2014). Near real time vegetation monitoring at global scale. *IEEE Journal of Selected Topics in Applied Earth Observations and Remote Sensing, 7*, 3473-3481

Verger, A., Baret, F., Weiss, M., Filella, I., & Peñuelas, J. (2015). GEOCLIM: A global climatology of LAI, FAPAR, and FCOVER from VEGETATION observations for 1999–2010. *Remote Sensing of Environment, 166*, 126-137

Verger, A., Baret , F., Weiss, M., Kandasamy, S., & Vermote, E. (2013). The CACAO method for smoothing, gap filling and characterizing seasonal anomalies in satellite time series. *IEEE transactions on Geoscience and Remote Sensing, 51*, 1963-1972

Vermote, E., & Claverie, M. (2013). Climate Algorithm Theoretical Basis Document. AVHRR Land Bundle - Surface Reflectance and Normalized Difference Vegetation Index. In (p. 38): NOAA

Vermote, E., Justice, C., Csiszar, I., Eidenshink, J., Mynemi, R., Baret, F., Masuoka, E., & Wolfe, R. (2010). A terrestrial surface climate data record for global change studies. In J. Sobrino (Ed.), *Third International Symposium on Recent Advances in Quantitative Remote Sensing*. Torrent (Spain)

Vermote, E., Justice, C., Csiszar, I., Eidenshink, J., Myneni, R., Baret, F., Masuoka, E., & Wolfe, R. (2009). A Terrestrial Surface Climate Data Record for Global Change Studies. In, *Fall Meeting, San-Francisco (USA)*: Eos Transactions, Suppl., v. 90, no. 52: Washington, D.C., American Geophysical Union, abstract number IN42A-08. (Also available online at http://www.agu.org/meetings/fm09/waisfm09adv.html.)

Vermote, E., & Kaufman, J.K. (1995). Absolute calibration of AVHRR visible and near-infrared channels using ocean and cloud views. *International Journal of Remote Sensing, 16*, 2317-2340

Weiss, M., Baret, F., Myneni, R., Pragnère, A., & Knyazikhin, Y. (2000). Investigation of a model inversion technique for the estimation of crop charcteristics from spectral and directional reflectance data. *Agronomie, 20*, 3-22

ANNEX 1: GEOCLIM, A CLIMATOLOGY OF GEOV1 LAI, FAPAR AND FCOVER

The principles of the generation of the GEOCLIM dataset are here described (Figure 9). Further information is provided in Verger et al. (2015).

Inter-annual average values from the GEOV1 Copernicus Global Land time series of biophysical LAI, FAPAR and FCOVER at 1-km resolution and 10-day frequency were first computed for 1999 to 2010 (Baret et al. 2010). Since the climatology plays an important role for gap filling and temporal smoothing of the data, possible artifacts in the climatology were corrected through a two-step process:

- Correction of specific artifacts
- Gap filling and temporal smoothing

Correction of specific artifacts

The climatology was first corrected over specific problematic conditions (Figure 9) based on the prior knowledge:

- Some artifacts are observed at ***northern high latitudes during the winter time when the sun zenith angle, SZA>70º***: Anomalous seasonality and unexpected increases in LAI (FAPAR, FCOVER) with an artificial maximum peak in winter and high inter-annual variability. These artefacts mainly due to snow cover or very poor illumination conditions that limited the number of valid observations and the reliability of the bidirectional reflectance model applied for the correction of VEGETATION data (Roujean et al. 1992). The LAI (FAPAR, FCOVER) values are expected to be relatively stable and low due to the low temperatures, short days, and low illumination during winter at these high latitudes. To correct these artefacts at northern high latitudes (latitude>40º) for winter (defined here as the period for which the *sun zenith angle, SZA>70º),* the climatology values higher than the 20-percentile ($P20^{clim}$) were fixed at minima by preferentially selecting the values computed from at least three valid observations. If none of the dekads meets this condition, the minimum value computed over all the dekads was used.
- Significant artifacts were also detected in ***Equatorial and tropical latitudes*** due to the permanent presence of clouds which results in high instabilities in the temporal profiles of GEOV1/VGT climatology. Since most of these cases correspond to evergreen broadleaf forests (EBF), a minimum seasonality and high values were assumed. A pixel was identified as being an EBF if the 90-percentile ($P90^{clim}$) of LAI climatology is > 4.5 and the 20-percentile $P20^{clim}$ is $>P90^{clim}$ -1.5. This method for the detection of EBF is based only on GEOV1 products (Figure 10a): it agrees well with the GLOBCOVER land-cover map (Defourny et al. 2009) (Figure 10b). For EBFs, the climatology values were fixed to the 90-percentile. A quality flag indicating that the pixel was identified as EBF is activated (QF_{EBF}=1). It is subsequently used in Steps 1-4 of Branch B.
- Some artifacts were also detected in GEOV1/VGT climatology for ***bare soil (BS) areas.*** A pixel was identified as being a BS if the 90-percentile of LAI climatology $P90^{clim}$ is <0.05. For those cases the climatology values were fixed to the median value (50-percentile)

computed over the entire period. In addition, a quality flag indicating that the pixel was identified as BS is activated (QF_{BS}=1). It is subsequently used in Step 4 of Branch B.

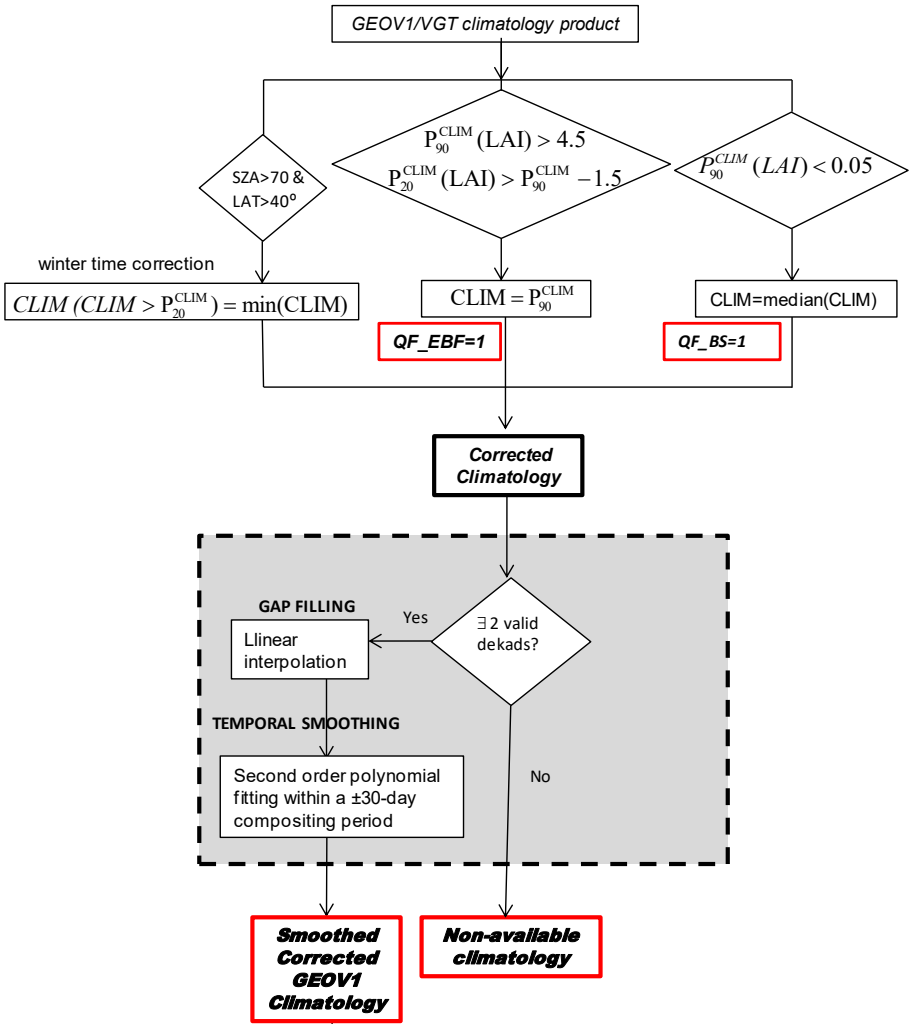

Figure 9: Flow chart showing how the GEOV1/VGT climatology is corrected from residual artifacts.

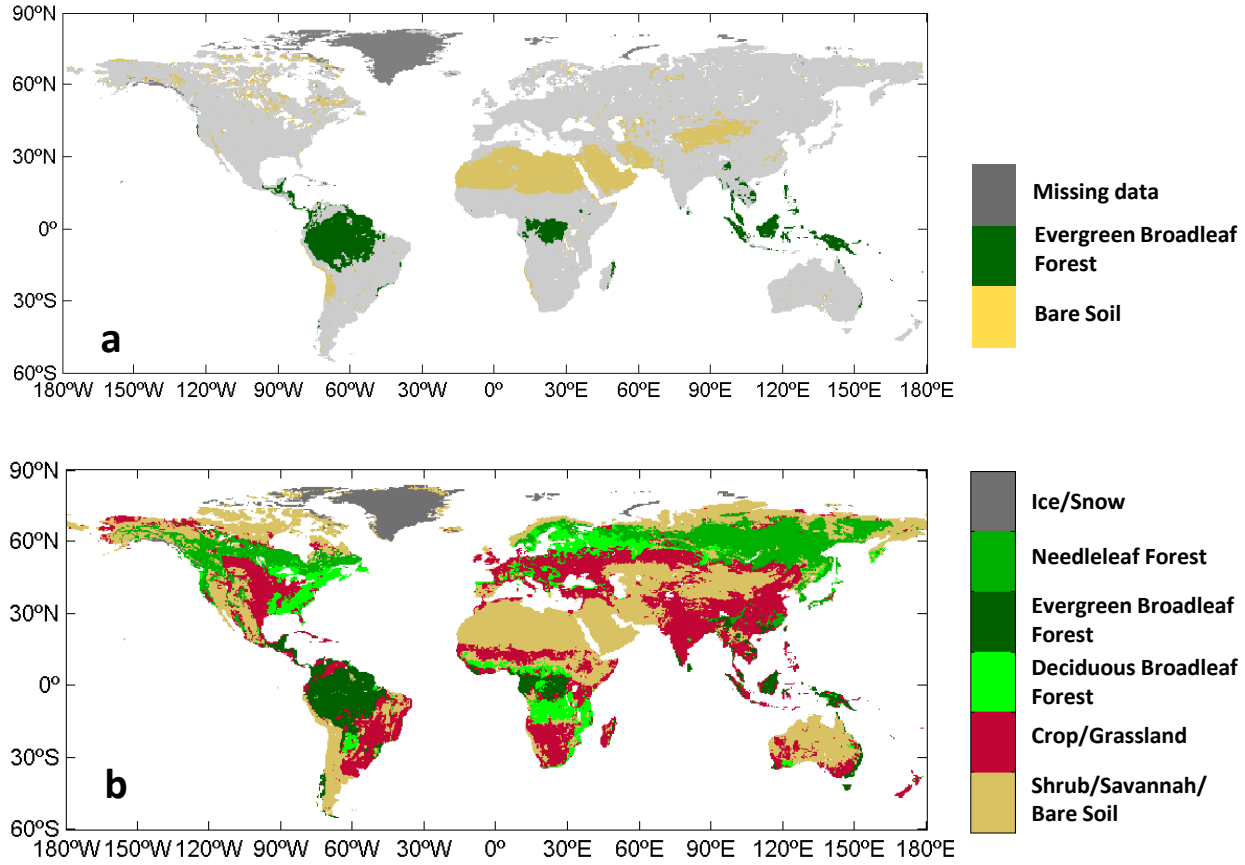

Figure 10: (a) Map of bare soil and evergreen broadleaf forest areas identified based on GEOV1/VGT climatology. (b) Simplified GLOBCOVER land-cover map after aggregating the 22 original classes into six main land-cover classes.

Gap filling and smoothing

The climatology was then gap filled and smoothed to eliminate possible high temporal frequency residual artifacts. The gap filling (GF) and temporal smoothing (TS) techniques proposed by (Verger et al. 2011) were applied here.

- ***Gap filling.*** A simple linear interpolation was applied if two valid dekads are available along the 36 potential dekads of the climatology
- ***Temporal smoothing.*** A second order polynomial order was fit to the data within a ±30-day compositing period centered on the date being smoothed. This polynomial fitting applied at a dekadal time step.

Figure 11 shows the original and corrected climatology at four problematic sites.

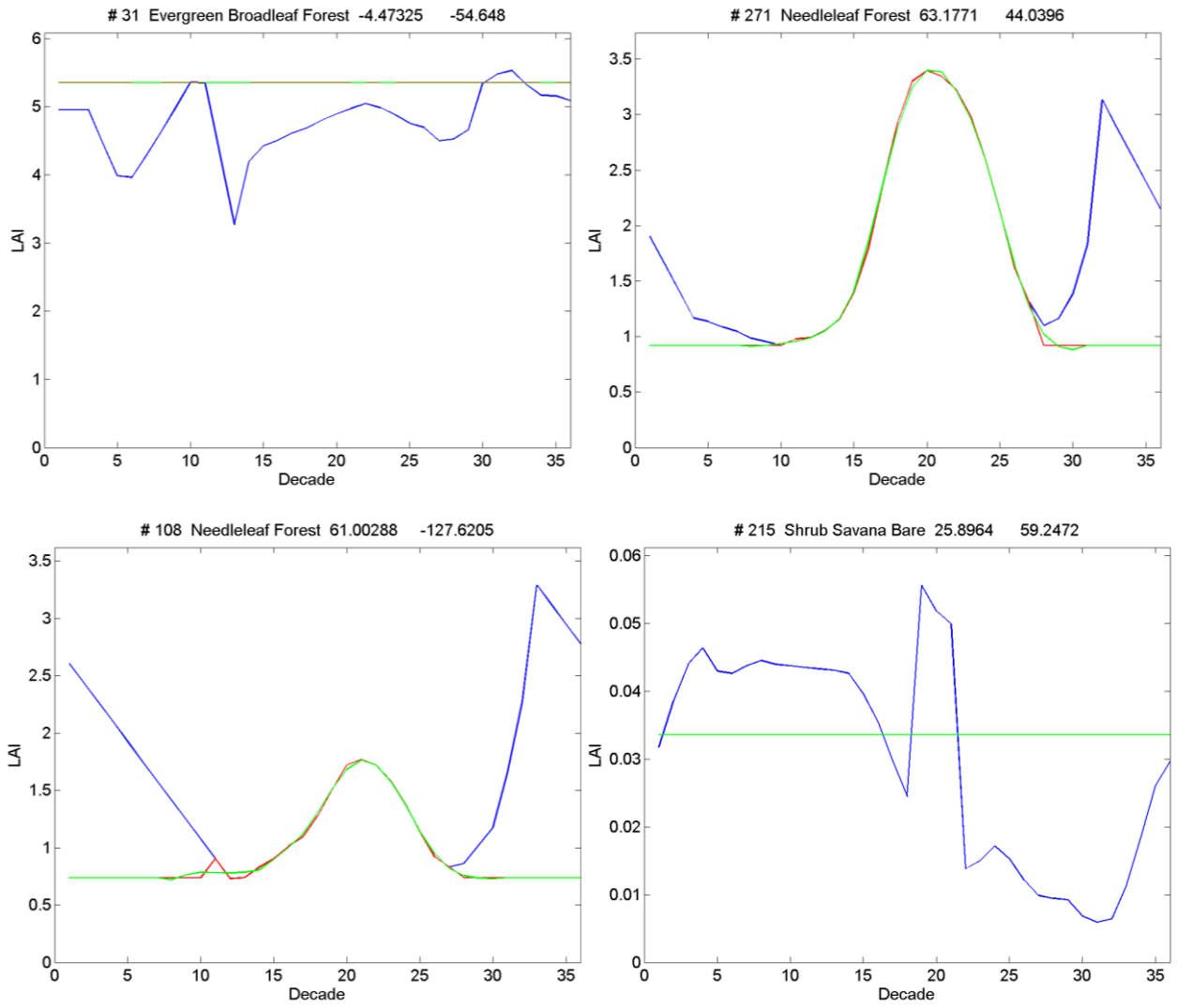

Figure 11: Correction of GEOV1/VGT climatology. The blue line corresponds to the original GEOV1/VGT climatology LAI product. The red line corresponds to the corrected climatology based on prior knowledge. Green line is the final GEOCLIM climatology resulting from applying gap filling and temporal smoothing techniques to the first corrected climatology.

ANNEX 2: NEURAL NETWORKS CALIBRATION

BUILDING THE LEARNING DATA SET

The neural networks were calibrated using the LTDR4 BELMANIP2 sites extracts over the 2003-2007 period, that includes acquisitions from both NOAA16 and NOAA18. The BELMANIP2 set of sites is an update of the original BELMANIP sites (Baret et al., 2006). The 445 BELMANIP2 sites present the same distribution of vegetation types and conditions as the Earth's surface while showing little topography and good level of homogeneity. The land cover homogeneity of each site was double checked using the GLOBCOVER map, and the Google Earth engine (Weiss et al., 2014). Figure 12 shows that at 3km resolution almost 90% of the sites are homogeneous in terms of land cover.

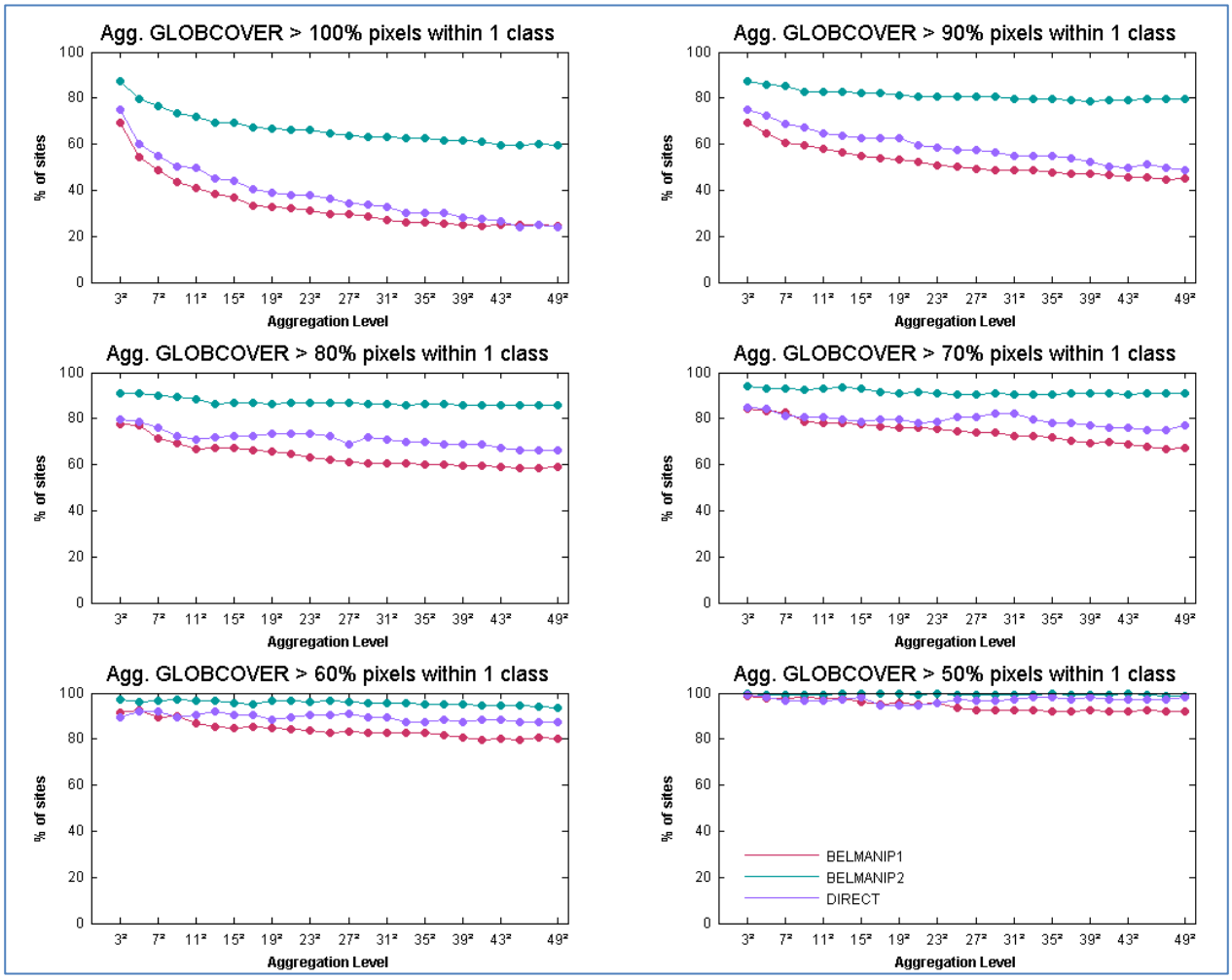

Figure 12. Homogeneity of the BELMANIP2 sites (as compared to BELMANIP1 and DIRECT validation site) at different spatial resolution (from 3 to 49km²).

The inputs of the neural networks are LTDRV4 surface reflectance in the red and near infrared bands as well as the cosine of the sun zenith angle at 10:00 solar time for FAPAR.

To keep the consistency with the GEOV2-CGLS product, the neural networks were calibrated with the same output, i.e. a product resulting from the fusion of MODIS and CYCLOPES. To generate the training data base, all the inputs (reflectance) and outputs (products) should share the same spatial and temporal support. For this purpose, MODIS products were re-projected into the CYCLOPES system (latitude/longitude on WGS-84, E.G plate carrée projection at 1/112°). We used 3x3 pixels extracts. As LTDR data are generated daily while MODIS and CYCLOPES correspond to a synthesis of 8 and 10 days products, the training dataset is generated with a dedicated processing:

1. Selection of the MODIS products: all the MODIS products available within ±10 days around the LTDR-AVHRR date are gathered. Then, only the main and main + saturation LAI and FAPAR products are considered. This will result in nMOD available products (0<nMOD<18)
2. Selection of CYCLOPES products: products available within ±10 days around the LTDR-AVHRR date are gathered. Only the valid LAI, FAPAR and FCOVER products are considered. This results in nCYC products (0<nCYC<9) .
3. If there are at least 5 valid products for MODIS and CYCLOPES (nMOD>4 and nCYC>4):
    a. If the majority of BELMANIP2 site pixels is not classified as an EBF (GLOBCOVER Classification), we compute the median of the CYLOPES and the median of the MODIS product.
    b. If the majority of BELMANIP2 site pixels is classified as an EBF (GLOBCOVER Classification), this potentially indicates a high level of noise in the data since these biomes are located in very cloudy areas. We compute the difference δMOD between the 70% and 90% percentiles within the nMOD MODIS product value. If δMOD <0.2 then the following three values are computed:
        i. The 70% percentile value of LAI and FAPAR products is computed over the nCYC products available.
        ii. The 70% percentile value of LAI and FAPAR products is computed over the nMOD products available. The several threshold values were defined after trial and error tests to reduce the large variability observed over the individual MODIS LAI and FAPAR values and get more consistency between MODIS and CYCLOPES products. The first condition on δ_{MOD} over LAI MODIS products prevents from using too variable values, while the lower values may show higher variability because of possible cloud contamination or atmospheric residual effects. Similarly, the 70% percentile value selected for LAI and FAPAR reduces the occurrence of cloud and atmosphere artifacts.
4. As already proposed for the GEOV2 products, we used a fused product between the resulting daily CYCLOPES and MODIS values to benefit from the better performances observed for CYCLOPES FAPAR products for the lower FAPAR values (no offset for the low values), and for MODIS LAI products for the larger LAI values. We thus averaged MODIS and CYCLOPES products using a weighing factor (Figure 13):

$$w = \frac{1}{0.982}\left(1 - \frac{1}{(1 + \exp(-2.LAI_{CYCV31} + 4))}\right)$$

$$\begin{cases} LAI_{fused} = LAI_{MODC5}.(1-w) + LAI_{CYCV31} \cdot w \\ fAPAR_{fused} = fAPAR_{MODC5} \cdot (1-w) + fAPAR_{CYCV31} \cdot w \end{cases} \quad [2]$$

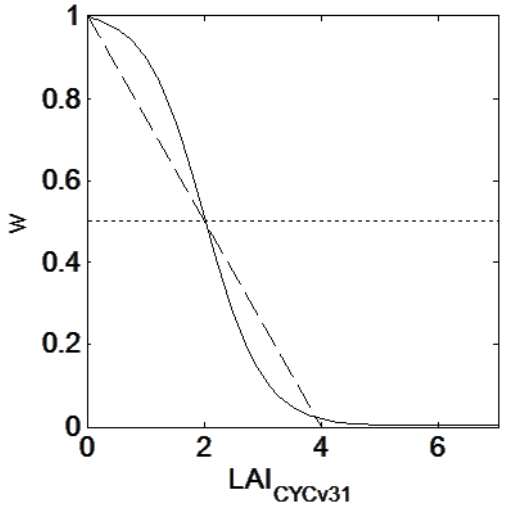

Figure 13. The weighing function used in GEOV2 AVHRR_LTDR4 for the fusion between CYCLOPES and MODIS LAI and FAPAR products. The dashed line corresponds to the weight used for generating GEOV1 products. The dotted line corresponds to w=0.5.

For FCOVER, we used the CYCLOPES product which is the only one available for the considered period. In a similar way as was done for the GEOV1 product (Baret et al, 2013), we rescaled the CYCLOPES product as:

$$FCOVER = \frac{FCOVER}{0.69} \quad [3]$$

FILTERING OUT THE NNT LEARNING DATABASE

We selected solely the data of best quality for AVHRR based on their associated flags (e.g. data for which the cloud, cloud shadow, sunglint and invalid red or NIR reflectances are not activated). As they are still contaminated with noise, mainly due to cloud mis-detection or atmospheric residual effects, we have first applied different filters on the learning database to improve the estimation accuracy of the neural network.

Manual and visual filtering

We first filtered the AVHRR LTDR input reflectances. As red and NIR reflectances must be consistent to get a realistic product, we decided to train a first version of the neural networks with the AVHRR reflectances as inputs. We used a typical 2 layers architecture as used to generate GEOV2-CGLS

products: one hidden layer composed of 5 neurons characterized by a tangent sigmoid function and one output layer composed of one linear neuron. Inputs and output were normalized. The output (Product_0 at a daily time step) of the first neural net is computed in a similar way as for the final neural network by fusing CYCLOPES version 3.1 and MODIS collection 5 LAI.

The NNT was applied over the 2003-2007 period. The outliers in the daily Product_0 (first neural net) estimates were manually filtered out considering the GEOV1/VGT climatology as background information. The manual filtering was achieved using a graphical user interface specifically developed for that purpose. Considering that manual filtering is a tedious and time consuming task, we decided to perform the filtering only using the LAI product considering that the input bands are the same for the 3 variables and that the LAI/FAPAR/FCOVER time cycle are consistent between MODIS and CYCLOPES products. MODIS and CYCLOPES products were also manually filtered in the same manner and for the same period. We filtered only the temporal profile of the central pixel of the site, assuming that the surrounding pixels have the same behavior.

The temporal consistency was used here as the main criterion: the temporal profile should be more or less the same as the climatology (considering that the season can be shifted between years and the LAI level can be different) and the temporal profile should be smooth. Despite the inherent subjectivity associated to manual filtering, at this algorithm level, a manual method was preferred to automatic methods to avoid possible systematic biases which would affect neural networks estimates. Note however that manual filtering was only applied to the training database while completely automatic methods of outlier detection were applied in subsequent steps (step 2A, 4A, 1B and 3B) of the algorithm. The performance of this manual method is illustrated in Figure 14.

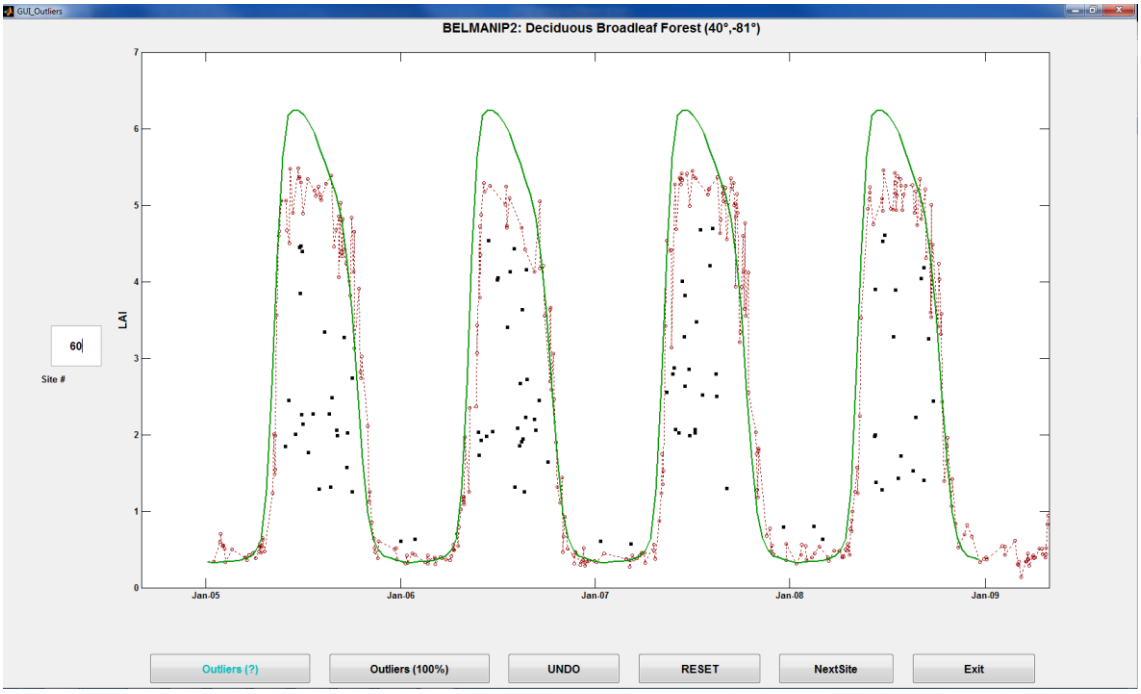

Figure 14: Manual filtering of the outliers. The green line corresponds to the GEOV1 climatology product, red circles to AVHRR-V0 (first neural net) valid data, black squares are outliers.

Filtering residual artefacts

As manual filtering might be not enough when a high level of noise and shaky temporal profiles are obtained for some of the BELMANIP2 sites, residual outliers were filtered.

We looked at the relationship between AVHRR LAI product V0 and AVHRR-NDVI (**Figure 15**). As expected, we observed an exponential relationship. The remaining outliers in the LAI-NDVI plane were finally removed by considering that all the values above and below two exponential curves between LAI and NDVI defined by equation 3 are outliers (**Figure 15**). The data that are selected for the learning data base follow:

$$\begin{cases} LAI_{FUSE} \leq e^{\frac{NDVI_{AVHRR}}{0.3}} - 0.85 \\ LAI_{FUSE} \geq e^{\frac{NDVI_{AVHRR}}{0.6}} - 1.7 \end{cases} \quad [4]$$

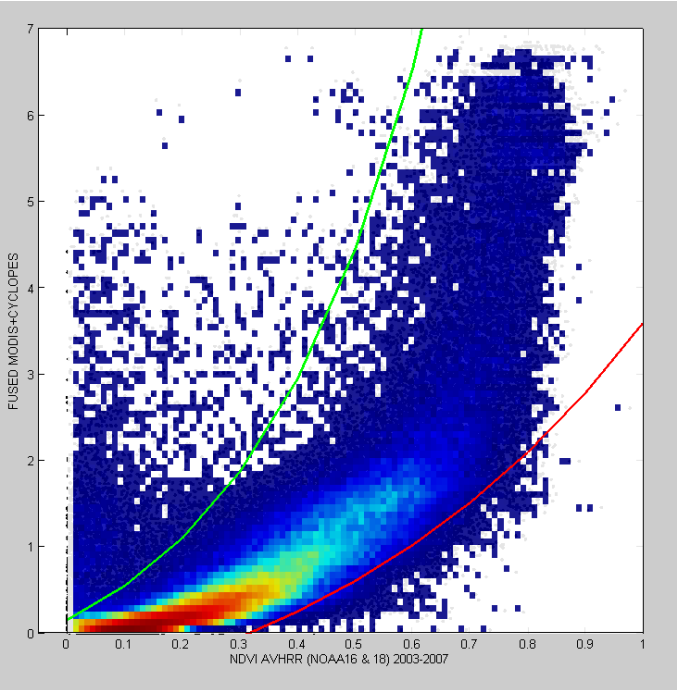

Figure 15: Filtering of outliers in the training dataset based on the LAI-NDVI relationship is displayed as a density plot: the redder, the denser the points are. The green and the red lines define the upper and lower limits

DETERMINATION OF THE DEFINITION DOMAIN

The performances of the neural network technique are closely linked to the way the learning database is generated. When applying them on a given pixel, it is necessary to check whether this

pixel is represented or not in the learning database. This will avoid applying the neural networks on residual clouds for example.

The RED/NIR relationship of the filtered learning database is presented in Figure 16 and shows that it is possible to define two curves between each we can ensure that the performances of the neural networks will not be degraded. The two curves are defined by:

$$\begin{aligned} &NIR \geq RED \\ &NIR \leq -2.41\, RED^3 + 4.32\, RED^2 - 1.16\, RED + 0.54 \ \text{if}\ RED < 0.685 \\ &NIR \leq 1\ if\ RED \geq 0.685 \end{aligned} \quad [5]$$

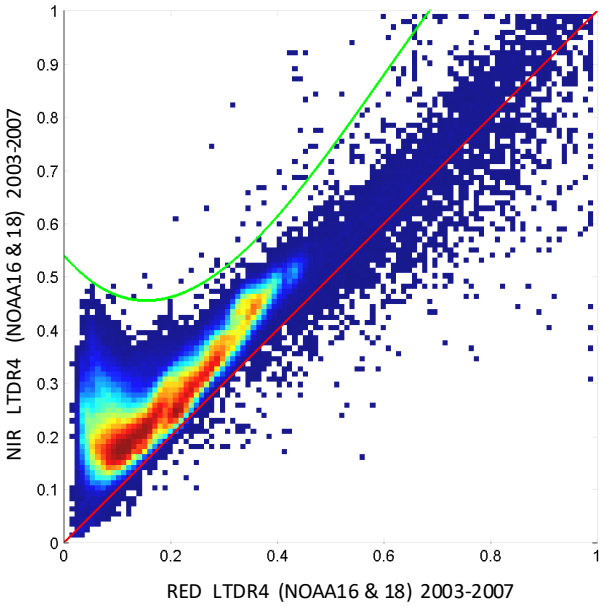

Figure 16: The two curves corresponding to the limits of the definition domain of the filtered learning database. Pixels are declared valid if they are between the green and red curve limits.

CALIBRATING THE NEURAL NETWORKS

Once the learning dataset is properly set up and filtered, we trained the neural networks to relate the AVHRR LTDRV4 reflectance to the fused CYCLOPES and MODIS products.

The training dataset was finally composed of 250 000 paired values of AVHRR reflectances and the corresponding FUSED variables. The whole dataset was randomly split into a learning dataset made of 70% of the data available, a validation dataset of 15% of samples to evaluate the theoretical performances and the remaining 15% are used to prevent possible overfitting during the training process.

Ten neural networks were trained in parallel for each variable. The ones achieving the best performances over the validation dataset were selected. The theoretical performances evaluated over the test dataset show a good predictive capacity of the neural networks for the three biophysical variables (Figure 17). Moreover, no obvious bias in the estimates is observed.

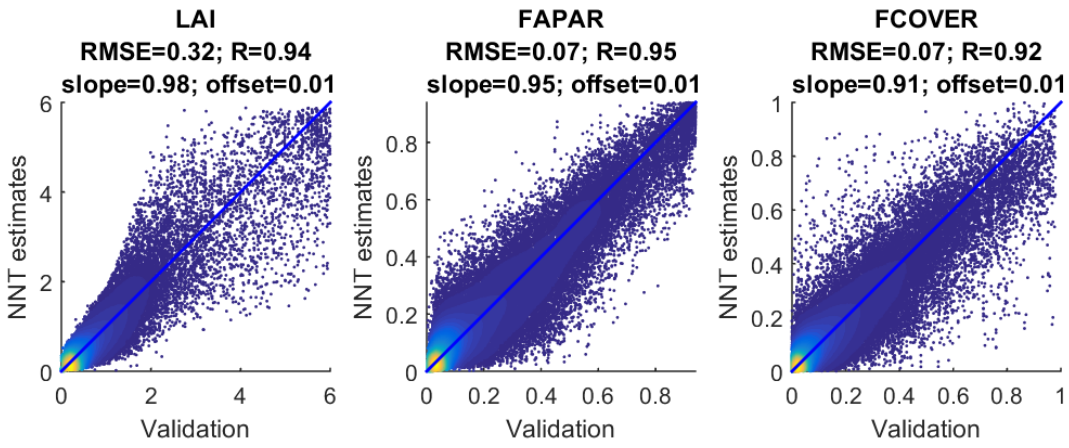

Figure 17: Theoretical performances of the neural network used to estimate LAI, FAPAR and FCOVER products over the validation data set (37500 samples) made of the fused CYCLOPES and MODIS products. The color indicates the density of points from red (highest) to blue (lowest density). RMSE is the root mean square error, R is the Pearson correlation coefficient, and slope and offset are the parameters of the least squares regression. The blue line is the 1:1 line.

PRACTICAL IMPLEMENTATION OF THE NNTS

All the parameters (normalization, synaptic coefficients and biases, polynomial rescaling) that define the neural network are provided in an Excel file associated to this ATBD.

To apply the neural network, the following steps must be followed:

- **Normalization of the inputs**: for all the inputs X (Red, Near infrared bands, and cosine of the solar zenith angle at 10:00 for FAPAR), the following normalization equation must be applied:

$$Xnorm = 2 \cdot (X - Xmin)/(Xmax - Xmin) - 1 \quad [6]$$

where $Xnorm$ is the normalized input value, and $Xmin$ and $Xmax$ are computed over the neural network training data set. Values of $Xmin$ and $Xmax$ will be provided in the excel sheet 'Normalization'.

- **Run the neural network.** The neural network is described by its architecture, *i.e*, the number of hidden layers (1) and the output layer (1). Each layer is described by its number of neurons, associated weight and biases and transfer function. For the neurons of the hidden layer (5 neurons), the transfer function is a tangent sigmoid function given by:

$$y = Tansig(x) = 2/(1 + exp(-2x)) - 1 \quad [7]$$

For the output layer (one neuron), the transfer function is linear $(y = x)$ For each neural network (one per product), tables are provided given the weight and biases for each neuron in an excel file under sheet 'Weights'.

- **Denormalisation of the output product *P*.** It simply consists in applying the inverse function used for input normalization:

$$P_{Step2A} = 0.5 \cdot (P_{norm}^{NNT} + 1) \cdot (P_{max}^{NNT} - P_{min}^{NNT}) + P_{min}^{NNT} \quad [8]$$

where $Pnorm$ is the normalized output value issued from the NNT, and P_{min}^{NNT} and P_{max}^{NNT} are the minimum and maximum value of the product computed over the neural network training data set. These values are described under excel sheet 'Normalization'.